# Chapter 3

# Wavefield extrapolation by linearly transformed wave equation

Many different-order approximations of the one-way scalar wave equation have been suggested for use in seismic imaging and modeling. Of these approximations, the first-order approximation, usually called the 15-degree equation, is most commonly used in industry. However, all these approximations break down when handling steep-dip, or wide-angle, events.

Through a linear transformation of the wave equation, the *LITWEQ* is obtainable, without approximation. The LITWEQ is in the form of the 15-degree equation. Its solution is still a two-way wave solution. By imposing the boundary condition for upcoming (or downgoing) waves, the LITWEQ can be applied to seismic imaging (or modeling). Implementing the LITWEQ with a finite-differencing algorithm gives an *all-dip,* finite-difference wave-extrapolation operator, which solves the angle limitation problem in conventional finite-difference methods. This new method is also more efficient than the Fourier domain wide-angle methods (e.g., phase shift and Stolt), in handling the problem of wavefield extrapolation in laterally inhomogeneous media.

In this chapter, the LITWEQ will be derived first for a constant-velocity medium and then for a velocity-varying medium. Each case will be illustrated by some computational examples.

## § 3.1 REVIEW OF CONVENTIONAL FINITE-DIFFERENCE MIGRATION

Most extrapolation methods used in seismic imaging (i.e., migration) and modeling are based upon wave-equation theory. For a two-dimensional (2-D) elastic earth model, the two-way scalar wave equation is of the following form:

$$\frac{\partial^2 P}{\partial x^2} + \frac{\partial^2 P}{\partial z^2} - \frac{1}{v^2}\,\frac{\partial^2 P}{\partial t^2} \;=\; 0\,, \tag{3.1}$$

where $P$ is the wavefield, $x$ is the horizontal coordinate, $z$ is depth, $t$ is time, and $v$

is velocity.

When solving the scalar wave equation (3.1), we must have not only the boundary, or initial, conditions of the wavefield itself, but also the boundary, or initial, conditions of the first $z$ derivatives of the wavefield. Unfortunately, these first derivatives are presently not recorded in routine seismic surveys.

To avoid the requirement of knowing the vertical derivatives in solving the two-way equation (3.1) and also to obtain only a one-way (either up or down) solution [according to the exploding reflector model (Loewenthal et al., 1978)], we can use the one-way scalar (square-root) wave equation:

$$\left\{ \frac{\partial}{\partial z} \pm \frac{1}{v} \frac{\partial}{\partial t} \left( 1 - v^2 \frac{\dfrac{\partial^2}{\partial x^2}}{\dfrac{\partial^2}{\partial t^2}} \right)^{1/2} \right\} P \;=\; 0 \,, \tag{3.2}$$

where the positive sign is used in modeling, the negative in migration, and the velocity is half of the true velocity. [From now on, it should be understood that the velocities used in the equations (in this thesis) that are based on the exploding reflector model are halves of the true velocities. True velocities will be used only when we discuss two-way wavefield extrapolations in chapters 4 and 5.]

However, while equation (3.2) eliminates the requirement of knowing the vertical derivatives of the wavefields, it contains a square-root-of-differentiation operator that cannot easily be implemented numerically.

Fourier-domain extrapolation algorithms, such as the phase shift (Gazdag, 1978) and Stolt (Stolt, 1978) methods, transform time-space-domain derivatives (inside the square-root operator) into Fourier-domain polynomials, so that the square-root-of-differentiation operator is then purely a scalar square-root operator. However, certain approximations (interpolations or stretches) have to be made in these methods when media velocities are not constant (Gazdag and Sguazzero, 1984; Stolt, 1978).

With approximation, algorithms in the time-space (or frequency-space) domain, such as finite-difference, expand the square-root operator to a finite number of terms (or a finite number of orders). Finite-difference methods also need lateral boundary conditions, such as absorbing boundary conditions, as well as natural boundary conditions, such as upcoming-wave boundary conditions.

The continued fraction expansion was first used by Muir to approximate the square-root operator, $R \;= \sqrt{1 - X^2}$, where $X^2 = v^2 \, \dfrac{\partial^2/\partial x^2}{\partial^2/\partial t^2}$. The expansion is

$$R_n = 1 - \frac{X^2}{1 + R_{n-1}} , \tag{3.3}$$

where $n$ is the order of approximation, and usually $R_0 = 1$ (Claerbout, 1985).

A Taylor series expansion of the square-root operator can also be used, though taking more than two terms in expansion will give computationally unstable schemes (Claerbout, 1985). The Taylor series expansion of the square-root operator is

$$R = 1 - \frac{v^2}{2} \frac{\frac{\partial^2}{\partial x^2}}{\frac{\partial^2}{\partial t^2}} + \textit{higher order terms} \cdots . \tag{3.4}$$

Using the first-iteration approximation ($n = 1$) in Muir's expansion, or dropping higher-order terms in the Taylor expansion (3.4), we get the first-order approximate equation for migration,

$$\left\{ \frac{\partial}{\partial z} - \frac{1}{v} \frac{\partial}{\partial t} \left( 1 - \frac{v^2}{2} \frac{\frac{\partial^2}{\partial x^2}}{\frac{\partial^2}{\partial t^2}} \right) \right\} P = 0 . \tag{3.5}$$

Upon applying the retarded-time coordinate transformation

$$\begin{cases} x' = x , \\ z' = z , \text{ and} \\ t' = t + z/v , \end{cases} \tag{3.6}$$

equation (3.5) finally becomes the commonly used 15-degree migration equation:

$$\left\{ \frac{\partial^2}{\partial z' \partial t'} + \frac{v}{2} \frac{\partial^2}{\partial x'^2} \right\} P = 0 . \tag{3.7}$$

Another way of getting this approximate equation for migration is to apply the retarded-time coordinate transformation (3.6) to the wave equation (3.1) (Claerbout, 1976; Stolt, 1978), resulting in

$$\left\{ \frac{\partial^2}{\partial x'^2} + \frac{2}{v} \frac{\partial^2}{\partial z' \partial t'} + \frac{\partial^2}{\partial z'^2} \right\} P = 0 . \tag{3.8}$$

Dropping out the second $z'$ derivative term gives equation (3.7).

All the approximate equations replace the total square-root operator in equation (3.2) with an operator of a finite number of differentiation terms and limited accuracy.

The leading error term for the operator approximation is proportional to a power of $\sin\theta$, where $\theta$ is the angle of wave propagation (the angle measured from the vertical axis). Therefore, algorithms based on these approximate equations are not accurate when applied to events with large propagating angles. Using higher-order approximations of the square-root operator increases accuracy in extrapolating events with large propagating angles. However, the computational cost increases significantly when these higher-order approximate equations (e.g., the splitting method) are implemented on a computer (Ma, 1982; and Jacobs, 1982).

In the next section, we will look for a nonsingular linear transformation of the coordinates that can transform the last two terms in equation (3.1) into a single cross-derivative term. The resulting equation will be

$$\left\{ \frac{\partial^2}{\partial x'^2} + a \frac{\partial^2}{\partial z' \partial t'} \right\} P = 0 , \tag{3.9}$$

where $a$ is a coefficient that depends on the transform and velocity $v$. This equation, without approximation, is valid for all events, regardless of their propagating angles.

## § 3.2 THE LINEARLY TRANSFORMED WAVE EQUATION

### The transformation

Comparing the acoustic wave equation (3.1) and the LITWEQ equation (3.9), we notice that the two differential operators, $\partial^2/\partial z^2$ and $(1/v^2)\partial^2/\partial t^2$, in equation (3.1) are replaced by a single operator, $a\,(\partial^2/\partial z' \partial t')$, in equation (3.9). This substitution can be accomplished by using the following family of transformations:

$$\begin{cases} x' = x , \\ z' = c_1 z + d_1 t , \text{ and} \\ t' = c_2 z + d_2 t , \end{cases} \tag{3.10}$$

where $c_1$, $c_2$, $d_1$ and $d_2$ are constants when the velocity is constant. (The transformations in velocity-varying media will be discussed later in this chapter.)

Substituting transformation (3.10) into the wave equation (3.1), we can determine the coefficients used in the linear transformation by equating the coefficients on the left sides of equations (3.1) and (3.9):

$$\begin{cases} c_1^2 - d_1^2/v^2 = 0 , \\ c_2^2 - d_2^2/v^2 = 0 , \text{ and} \\ 2c_1 c_2 - 2d_1 d_2/v^2 = a . \end{cases} \tag{3.11}$$

Equation (3.11) is a general constraint for the transform coefficients. When $c_1 = 1/\sqrt{2}$, $d_1 = -v/\sqrt{2}$, $c_2 = 1/(v\sqrt{2})$, and $d_2 = 1/\sqrt{2}$, a special form of the linear transformations (unitary when regarding $vt$ and $vt'$ as variables) takes the following form:

$$\begin{cases} x' = x \ ; \\ z' = \dfrac{1}{\sqrt{2}}(z - vt) \ , \text{ and} \\ t' = \dfrac{1}{\sqrt{2}}(z/v + t) \ . \end{cases} \tag{3.12}$$

The inverse transformation is

$$\begin{cases} x = x' \ , \\ z = \dfrac{1}{\sqrt{2}}(z' + vt') \ , \text{ and} \\ t = \dfrac{1}{\sqrt{2}}(t' - z'/v) \ . \end{cases} \tag{3.13}$$

The resulting equation is then

$$\frac{\partial^2 P}{\partial x'^2} + \frac{2}{v}\frac{\partial^2 P}{\partial z' \partial t'} = 0 \ . \tag{3.14}$$

Equation (3.14) has been exactly transformed from a scalar wave equation for a constant-velocity medium without dropping any terms; it is one form of the constant-velocity LITWEQ defined in equation (3.9). Therefore, there is no dip constraint when using equation (3.14) for wavefield extrapolation. The LITWEQ has the same format as the conventional 15-degree equation, and can easily be solved numerically on a computer.

A second, simpler derivation of the LITWEQ can be performed in the Fourier domain. The dispersion relation of the wave equation, by 3-D Fourier transformation of equation (3.1), is

$$k_x^2 + k_z^2 - \frac{\omega^2}{v^2} = 0 \ , \tag{3.15}$$

or, after factoring,

$$k_x^2 + (k_z + \frac{\omega}{v})(k_z - \frac{\omega}{v}) = 0 \ . \tag{3.16}$$

Letting

$$\begin{cases} k_{z_1} = k_z + \dfrac{\omega}{v} \ , \text{ and} \\ k_{z_2} = k_z - \dfrac{\omega}{v} \ , \end{cases} \tag{3.17}$$

we get the dispersion relation of the wave equation in $(k_{z_1}, k_{z_2}, k_x)$,

$$k_x^2 + k_{z_1} k_{z_2} = 0 . \tag{3.18}$$

Transforming equation (3.18) back to $(z_1, z_2, x)$, we obtain one form of the LITWEQ in equation (3.9) with $a = 1$.

**The two-way equation**

Since the LITWEQ is linearly transformed from the two-way wave equation, it has a two-way solution and handles both upcoming waves and downgoing waves. For poststack migration of upcoming waves, a certain wavefield boundary condition must be imposed to eliminate the downgoing waves. On the other hand, the two-way property of the LITWEQ method can be used in two-way modeling, overturned-reflection imaging and two-way prestack migration.

Let us study the cross-derivative terms in the LITWEQ and the 15-degree equation. When the wavefield is independent of the horizontal axis (vertically propagating waves) as in one-dimensional (1-D) wave propagation, both the LITWEQ and the 15-degree equation take the form

$$\frac{\partial^2 P}{\partial \xi \, \partial \eta} = 0 , \tag{3.19}$$

with the common solution

$$P = \Phi(\xi) + \Psi(\eta) . \tag{3.20}$$

For the LITWEQ case, $\xi = t + z/v$ and $\eta = t - z/v$. Equation (3.20) has both the upcoming wave solution $\Phi(\xi) = \Phi(t + z/v)$ and the downgoing wave solution $\Psi(\eta) = \Psi(t - z/v)$. Therefore, the 1-D LITWEQ is actually the 1-D characteristic wave equation used in classical mathematics (Berg and McGregor, 1966; also see Appendix 3). Computing numerical solutions along the characteristic directions of wave propagation is more accurate and stable than along any other directions (see Appendix 3). To suppress the downgoing wave solution, we choose the following boundary condition:

$$P \Big|_{t+z/v \, > \, T_{\max}} = 0 . \tag{3.21}$$

Then, the maximum depth where the wavefield can be recorded is $z_{\max} = vT_{\max}$. Analyzing wave propagation in a zero-offset section by the exploding reflector concept (Loewenthal et al., 1976), the wave generated at the any depth at $t = 0$ can only travel upwards ($z$ must decrease) as time increases, because of condition (3.21). In other words, in constant-velocity media, the LITWEQ method with the boundary condition

(3.21) has only one upcoming-wave solution. Therefore, condition (3.21) is the upcoming wave boundary condition, sometimes called the zero-bottom condition. We will discuss later how to suppress the downgoing-wave solution of the LITWEQ method in variable velocity media.

For the case of the 15-degree migration equation, the variables in equation (3.20) correspond to $\xi = t + z/v$ and $\eta = z$. The solution is

$$P = \Phi(t + z/v) + \Psi(z), \tag{3.22}$$

which is the sum of an upcoming wave solution $\Phi(t + z/v)$ and a time-independent function $\Psi(z)$. Therefore, the 15-degree migration equation eliminates the downgoing waves completely by dropping off the higher-order terms in the expansion of the square-root operator, while introducing an extra time-independent function into the solution. It can also be shown that imposing the zero-bottom condition (3.21) will eliminate the time-independent solution of the 15-degree equation.

In 2-D wave propagation, $P$ is also a function of $x$. The reasoning just given for decomposing $P$ into either an upcoming-wave solution or a downgoing-wave solution is valid for the 2-D case, when events are propagating with small angles (as in a flat-layered medium) and when no reverberations are taken into account (as in migrating primary reflections). Therefore, instead of extrapolating wavefields along their characteristic lines, as in the 1-D LITWEQ method, in the 2-D LITWEQ method we extrapolate them along the characteristic lines of the small-angle events, which are the ones most likely to be present in seismic sections. Large-angle events are extrapolated nearly along their characteristic lines, which is still better than extrapolating along lines far from the characteristic ones (along the either $z$ axis or the $t$ axis, for example).

Physically, wave propagation can be characterized by the LITWEQ if we rotate the coordinates $(vt, z)$ by 45 degrees. This rotation does not change the orthogonality of the coordinate system, while the retarded coordinate transform does change the orthogonality. With the rotated coordinates $(vt', z')$, the wavefield solution can be represented by the sum of two functions, with one function depending only on $(z', x')$ and the other depending only on $(t', x')$.

## § 3.3 FINITE-DIFFERENCE IMPLEMENTATION OF THE LITWEQ

An important decision in using finite-difference techniques is the choice of boundary conditions. In performing seismic migration, we start with surface data $P(t, z=0, x)$ and migrate to get an image $P(t=0, z, x)$, under the upcoming wave boundary condition $P(t, z, x)\Big|_{t+z/v>T_{\max}} = 0$.

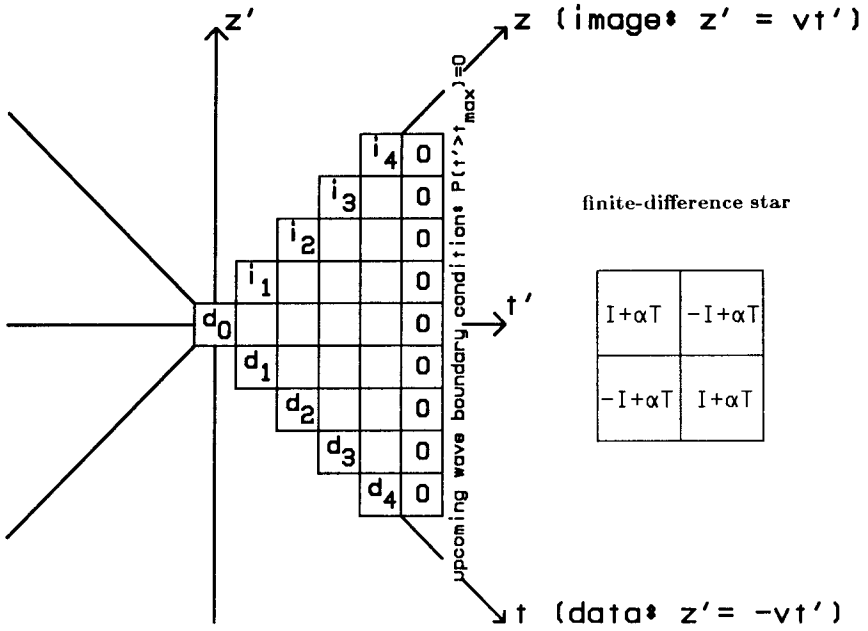


FIG. 3.1. Finite difference in $(t', z')$. The $x'$ axis is perpendicular to the $(t', z')$ plane. The length of data is assumed to be 5 in the figure. Data $P(x, z=0, t)$ is placed at $d_0, d_1, \ldots, d_4$. Image $P(x, z, t=0)$ is obtained at $d_0, i_1, \ldots, i_4$.

In the new LITWEQ coordinate system, $(t', z', x')$, the data are $P(t'=t/\sqrt{2}, z'=-vt/\sqrt{2}, x'=x)$; the image is $P(t'=z/(v\sqrt{2}), z'=z/\sqrt{2}, x'=x)$; and the upcoming-wave boundary condition is $P(t'>T_{\max}/\sqrt{2}, z', x') = 0$. Both the finite-difference grids and the four-point finite-difference star pattern of the LITWEQ, in the $(t', z')$ plane, are shown in Figure 3.1. The surface data lie at the line $z' = -vt'$, while the image lies along $z' = vt'$. The finite-difference star in the $(t', z')$ plane can move either up or to the left. With the upcoming-wave boundary condition, the data can be extrapolated from the $t$ axis to the $z$ axis to produce the image. Figure 3.1 is also valid when using the LITWEQ to do modeling; here causality conditions of the wavefield (with respect to both $t$ and $z$) should be used, instead of the

upcoming-wave boundary condition (see chapter 4).

From the viewpoint of numerical stability (Mitchell and Griffiths, 1980; Claerbout, 1985), the finite differencing in $x'$ is implicit, though an explicit scheme can be used too. The resulting implicit finite-difference representation of equation (3.14), in the $(t', z')$ plane, is

$$\left( \underset{\sim}{\mathrm{I}} + \alpha \underset{\sim}{\mathrm{T}} \right) \mathbf{P}_{t', z'+\Delta z'} = \left( \underset{\sim}{\mathrm{I}} - \alpha \underset{\sim}{\mathrm{T}} \right) \left\{ \mathbf{P}_{t', z'} + \mathbf{P}_{t'+\Delta t', z'+\Delta z'} \right\} - \left( \underset{\sim}{\mathrm{I}} + \alpha \underset{\sim}{\mathrm{T}} \right) \mathbf{P}_{t'+\Delta t', z'} , \tag{3.23}$$

where $\alpha = v \, \Delta t' \Delta z' / 8 \Delta x'^2$ , $\mathbf{P}$ is the wavefield vector along axis $x$ , $\underset{\sim}{\mathrm{I}}$ is an identity matrix, and $\underset{\sim}{\mathrm{T}}$ is a tridiagonal matrix with (–1, 2, –1) along its diagonal. The elements of the unknown vector on the left-hand side of equation (3.23) are given implicitly by the elements of the three known vectors on the right-hand side of the equation. For each step in moving the finite-differencing star in $(t', z')$, a tridiagonal, matrix-solver routine is called to get the wavefield along the whole $x'$ axis. The computer algorithm using equation (3.23) is unconditionally stable (Mitchell and Griffiths, 1980). Finite-differencing stars, in $(t', z')$ and $(x', z')$, used in the LITWEQ method, are shown in Figure 3.2. Because they use the same finite-difference star patterns, both the LITWEQ and the conventional 15-degree (Claerbout, 1976) methods have the same computational complexities.

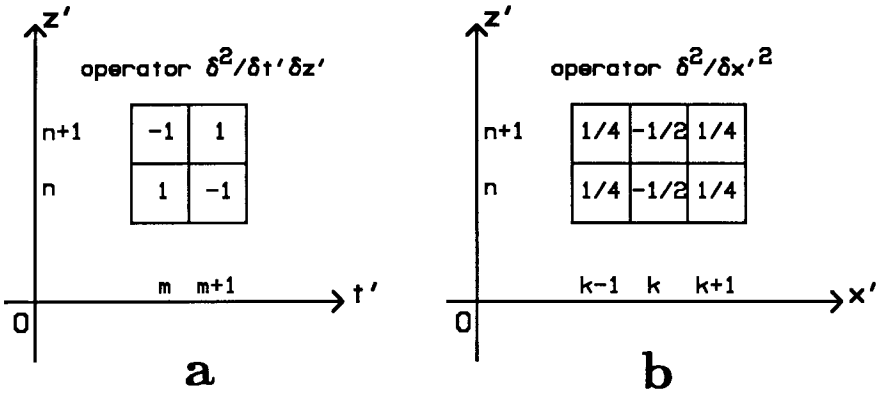


FIG. 3.2. **a.** Finite-differencing star of $\delta^2/\delta t' \delta z'$ in $(t', z')$. **b.** Finite-differencing star of $\delta^2/\delta x'^2$ in $(x', z')$. The operator $\delta^2/\delta x'^2$ has been averaged over the four elements in the $(t', z')$ plane. The finite-differencing star of $\delta^2/\delta x'^2$ in $(x', t')$ is the same as in $(x', z')$.

## § 3.4 EXAMPLES OF APPLYING LITWEQ MIGRATION TO SYNTHETIC DATA

### Impulse responses

Figure 3.3a shows the impulse response of the LITWEQ operator in a constant-velocity medium. The semicircle response is well preserved, which shows that the LITWEQ is valid for events of any propagating angle. For comparison, Figures 3.3b and 3.3c shows impulse responses of a 15-degree operator and a 45-degree operator, respectively. The steep-dip events corresponding to the upper part of the semicircle were distorted and eliminated by the low-pass-dipfiltering (low-pass) effect of the 15-degree and 45-degree migration operators.

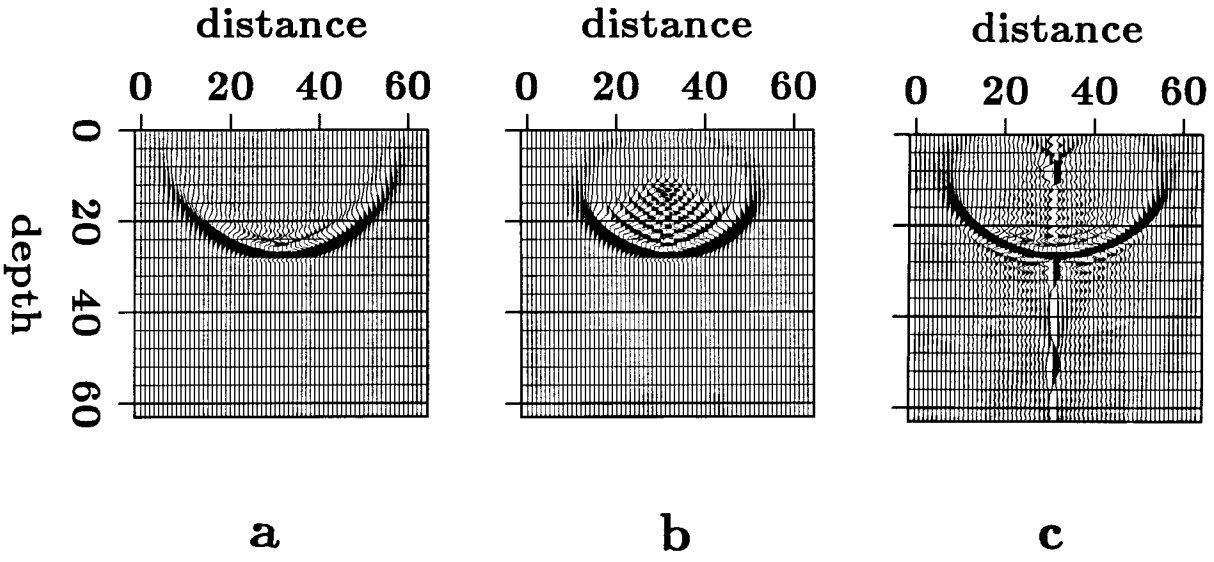


FIG. 3.3. **a.** Impulse response of the LITWEQ operator in a constant-velocity medium. The semicircle response shows the LITWEQ is accurate for any angles of propagating events. **b.** Impulse response of a 15-degree wave-equation operator. The operator locates correctly only the small-angle parts of the semicircle, while distorting the steep-dip parts. **c.** Impulse response of a 45-degree wave-equation operator. The operator gives better image of the semicircle than the 15-degree operator, but it fails to image the steep-dip parts.

**Imaging reflectors of different angles**

Figures 3.4a-3.4f compare the results of applying different migration operators to a synthetic dataset. The original model is composed of five segments of lines having five different dipping angles in a constant-velocity medium. The zero-offset record is generated by phase shift modeling. The four different migration operators are (1) 15-degree in the time-space domain; (2) 15-degree in the frequency-space domain; (3) 45-degree in the frequency-space domain; and (4) the LITWEQ. While small-angle reflectors are imaged well by all four methods, the reflectors with large angles, especially the steepest one, are well imaged only by the LITWEQ operator.

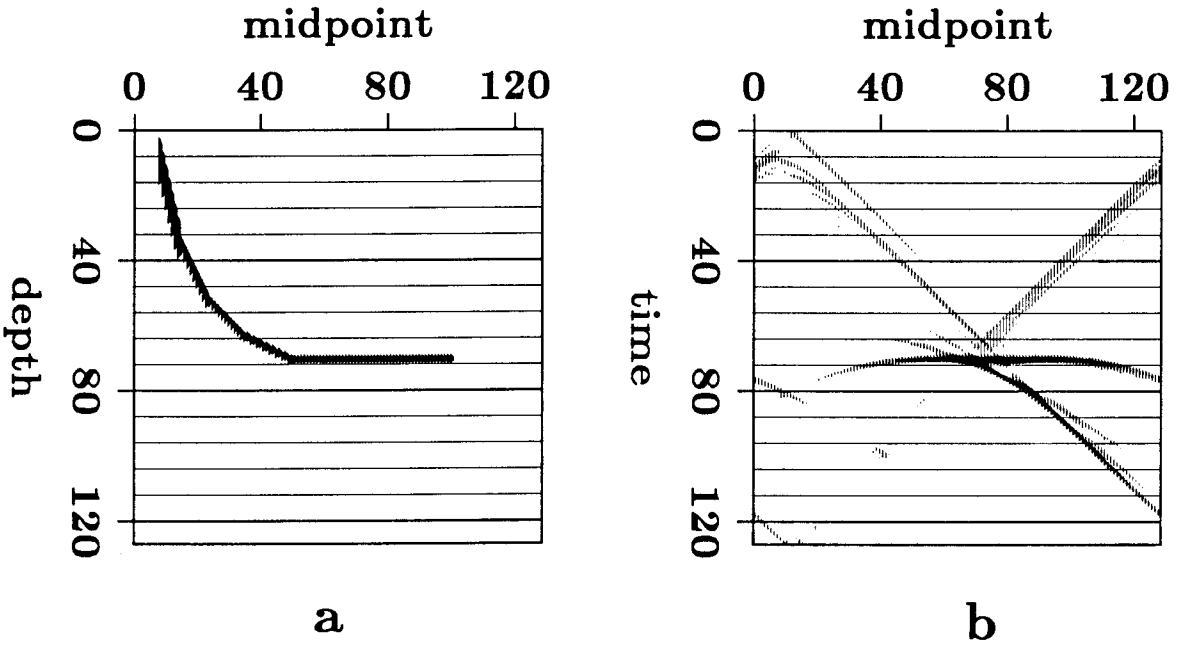


FIG. 3.4. **a.** The five-segment dipping-bed model. The velocity of the model is constant. The slopes of the five segments are 0, 0.5, 1, 2 and 4, respectively. The steepest one is about 76 degrees. Velocity is constant in the model. **b.** The synthetic seismogram generated with phase-shift modeling.

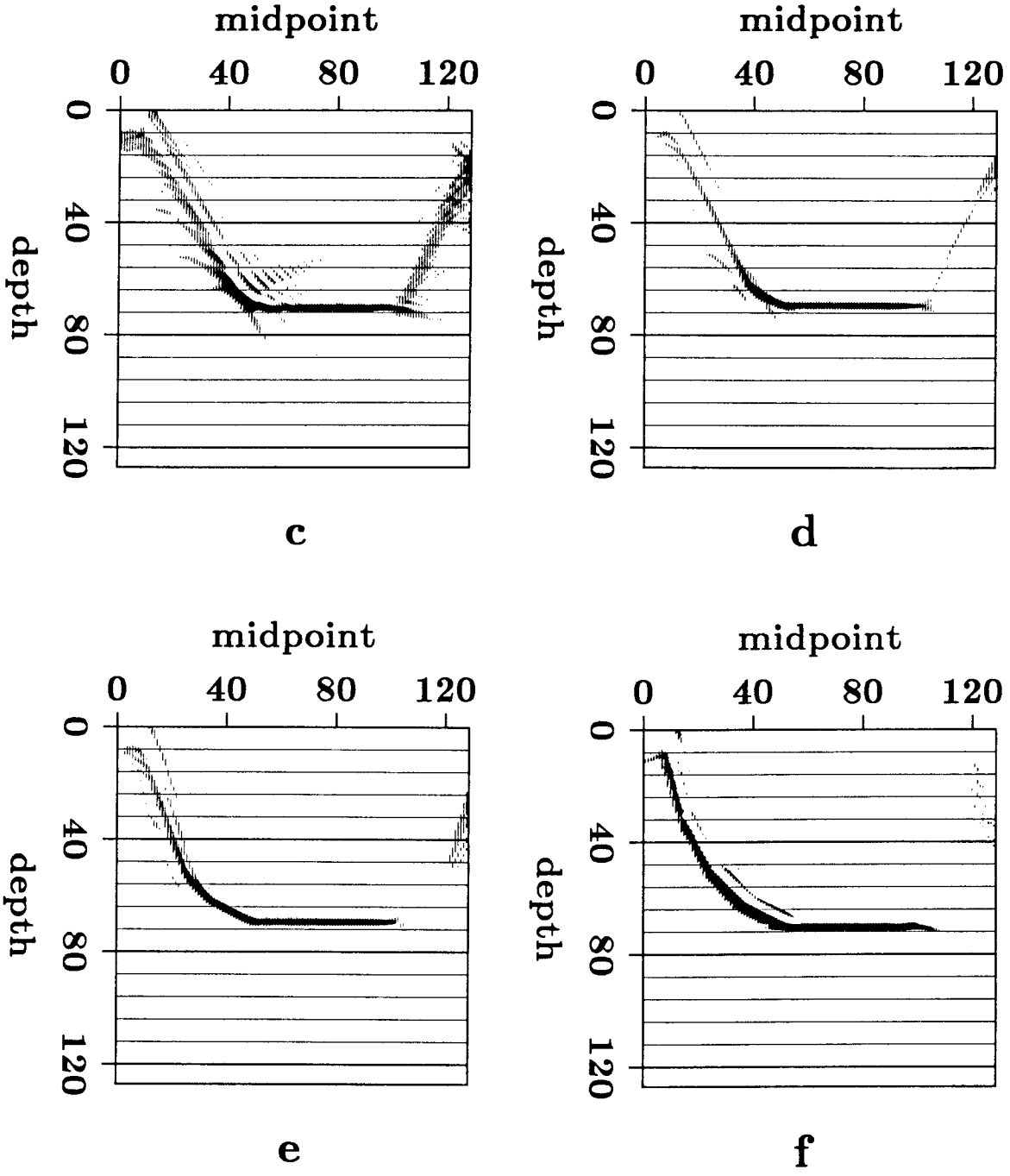


FIG. 3.4. **c.** Migration with the 15-degree operator in the time-space domain. **d.** Migration with the 15-degree operator in the frequency-space domain. **e.** Migration with the 45-degree operator in the frequency-space domain. **f.** Migration with the LITWEQ operator. All dipping reflectors are imaged well using the LITWEQ method.

## § 3.5 THE LITWEQ IN VARIABLE VELOCITY MEDIA

So far, we have not taken into account variation of the velocity $v$. When the velocity is varying, there will be some extra terms in the LITWEQ; similar extra terms also exist in other migration methods when the velocity is varying. When the velocity gradient is small and the extra terms are ignored, we can start with initial data $P(t, z=0, x)$ and use a velocity function $v(x, z)$ to do LITWEQ migration. However, the sampling intervals in the transformed domain are not constant when the migration velocity is a function of depth. To produce uniformly spaced grids in the transformed coordinates, the LITWEQ migration must start with initial data $P(t, \tau=0, x)$ and use some transformed velocity in the $(x, \tau)$ domain, where $\tau$ is called the pseudo-depth (related to the true depth $z$ by the transformed velocity).

### Derivation of the LITWEQ for variable velocity media

To derive the LITWEQ method for variable velocity media, let us first write the 2-D scalar wave equation for variable velocity media,

$$\frac{\partial^2 P}{\partial x^2} + \frac{\partial^2 P}{\partial z^2} - \frac{1}{v^2(x,z)} \frac{\partial^2 P}{\partial t^2} = 0 . \tag{3.24}$$

Define a depth-to-time transform:

$$\begin{cases} \tau = \int_0^z d\varsigma / v(x, \varsigma) \quad \text{and,} \\ x' = x , \end{cases} \tag{3.25}$$

and its corresponding time-to-depth transform:

$$\begin{cases} z = \int_0^\tau v_r(x', s)\, ds \quad \text{and,} \\ x = x' , \end{cases} \tag{3.26}$$

where $v_r(x', \tau)$ is the velocity transformed from $v(x, z)$ via equation (3.25) and $\tau$ is called the pseudo-depth (or two-way vertical time). The wave equation in $(t, \tau, x')$ is then

$$\frac{\partial^2 P}{\partial x'^2} + \frac{1}{v_r^2(x', \tau)} \left( \frac{\partial^2 P}{\partial \tau^2} - \frac{\partial^2 P}{\partial t^2} \right) = R , \tag{3.27}$$

where $R$ is given by

$$R = \frac{1}{v_r^3(x', \tau)} \frac{\partial v_r(x', \tau)}{\partial \tau} \frac{\partial P}{\partial \tau} - [\frac{\partial T_r(x', \tau)}{\partial x'} + T_r(x', \tau) \frac{\partial T_r(x', \tau)}{\partial \tau}] \frac{\partial P}{\partial \tau}$$

$$- T_r^2(x', \tau) \frac{\partial^2 P}{\partial \tau^2} - 2 T_r(x', \tau) \frac{\partial^2 P}{\partial x' \partial \tau} , \qquad (3.28)$$

and $T_r(x', \tau)$ is transformed from $T(x, z)$ that is defined by $T(x, z) = \frac{\partial \tau}{\partial x} = -\int_0^z \frac{\partial v(x, \varsigma)/\partial x \; d\varsigma}{v^2(x, \varsigma)}$.

The main reason for transforming the scalar wave equation (3.24) in $(t, z, x)$ to equation (3.27) in $(t, \tau, x')$ is to apply a velocity-independent linear transformation that will produce a LITWEQ method that has uniformly spaced intervals in its linearly transformed new coordinates. A second, also important reason, as will be explained later, is that we can suppress the reverberation artifacts caused by the two-way property of the migration operator and sharp changes in input migration velocity profiles, by ignoring the term on the right-hand side of equation (3.27). In variable velocity media, the transformation of coordinates $(t, z)$ to $(t', z')$ in section 3.2 will give a LITWEQ method with irregularly spaced intervals in $(t', z')$, since the transformation depends on velocity [equation (3.13)]. Equation (3.27) allows us to apply the *velocity-independent* linear transform,

$$\begin{cases} t_1 = \frac{1}{\sqrt{2}} (\tau + t) , \text{ and} \\ t_2 = \frac{1}{\sqrt{2}} (\tau - t) , \end{cases} \qquad (3.29)$$

resulting in

$$\frac{\partial^2 P}{\partial x'^2} + \frac{2}{\overline{v}_r^2(x', t_1, t_2)} \frac{\partial^2 P}{\partial t_1 \partial t_2} = \overline{R} . \qquad (3.30)$$

where $\overline{v}_r(x', t_1, t_2) = v_r[x', \tau = (t_1 + t_2)/\sqrt{2}]$ and $\overline{R}$ is transformed from $R$. In the transformed coordinates $(t_1, t_2)$, we now have uniformly-spaced intervals along both axes $t_1$ and $t_2$.

Because the $R$ term in equation (3.28) is proportional to both lateral and vertical velocity gradients, ignoring this term will have the advantage of suppressing reverberation artifacts generated at velocity discontinuities, though some care must be taken when velocity varies laterally. Some synthetic examples show that the LITWEQ method without the $R$ term are still kinematically correct, when velocity varies

smoothly along the $x$ direction.

When strong lateral velocity variations are present in a section, some terms (especially the last two terms) of $R$ in the right-hand side of equation (3.28) should be taken into consideration. As many other finite-difference methods, the severe lateral velocity variation will make the second-order finite-difference solution to the LITWEQ defined in equation (3.30) become unstable.

In case of very strong lateral velocity variations, another approach similar to Hatton's wave-theoretical depth migration (Hatton et al., 1981) can also be taken. Introducing a "$x$-independent" reference velocity $\overline{v}(z)$, for example,

$$\frac{1}{\overline{v}^2(z)} = \frac{\sum_{ix=1}^{nx} \frac{1}{v^2(ix, z)}}{nx}, \tag{3.31}$$

where $nx$ is the number of grid points in the $x$ direction, we can rewrite equation (3.24) as

$$\frac{\partial^2 P}{\partial x^2} + \frac{\partial^2 P}{\partial z^2} - \frac{1}{\overline{v}^2(z)} \frac{\partial^2 P}{\partial t^2} = \left[ \frac{1}{v^2(x, z)} - \frac{1}{\overline{v}^2(z)} \right] \frac{\partial^2 P}{\partial t^2}. \tag{3.32}$$

Now, letting $\tau = \int_0^z d\varsigma / \overline{v}(\varsigma)$ [or $z = \int_0^\tau v_r(\xi) d\xi$], where $v_r(\tau)$ is a reference $\tau$-dependent velocity transformed from $\overline{v}(z)$, the wave equation in $(t, \tau, x)$ is then

$$\frac{\partial^2 P}{\partial x^2} + \frac{1}{v_r^2(\tau)} \left( \frac{\partial^2 P}{\partial \tau^2} - \frac{\partial^2 P}{\partial t^2} \right) = \frac{1}{v_r^3(\tau)} \frac{\partial v_r(\tau)}{\partial \tau} \frac{\partial P}{\partial \tau} + \left[ \frac{1}{v_R^2(x, \tau)} - \frac{1}{v_r^2(\tau)} \right] \frac{\partial^2 P}{\partial t^2}, \tag{3.33}$$

where $v_R(x, \tau)$ is obtained from $v(x, z)$ by transforming $z$ to $\tau$. Now, we can apply the velocity-independent transformation (3.29) to equation (3.33) and obtain another LITWEQ for variable velocity media. Splitting of diffraction and time-shifting equations can then be applied to solve the new LITWEQ equation, as similar to the approach of Hatton et al.

**Reverberations**

Equation (3.30) is the LITWEQ representation of the scalar wave equation in variable velocity media. The term on the right-hand side of equations (3.30) is, when $v = v(z)$,

$$\overline{R} = R = \frac{1}{v_r{}^3(\tau)} \frac{\partial v_r(\tau)}{\partial \tau} \frac{\partial P}{\partial \tau} = \frac{1}{v(z)} \frac{\partial v(z)}{\partial z} \frac{\partial P}{\partial z} . \qquad (3.34)$$

Hence, in media with vertically-varying velocity, the term, $R$, is proportional to the vertical velocity gradient divided by the velocity, times the vertical wavefield gradient. Let us call this term the *reverberation* term, because it is proportional to the reflection coefficient [for normal (perpendicular to $z$) incidence] defined by $\Delta v / v$ in an acoustic medium where density is assumed to be constant. For finite-difference implementation of the LITWEQ method in media with vertically varying velocity we use the same four-point star pattern in $(t_1, t_2)$ as we use in constant-velocity media. The reverberation term in the right-hand side of equation (3.30), when $v = v(z)$, can be easily coded into the LITWEQ operator. The reverberation term is significant in modeling both reflections and reverberations. Because the velocity of the medium usually changes smoothly, we can neglect the reverberation term in most LITWEQ migrations. The reverberation term must be neglected if one is interested in migrating primary reflections only. Because it is proportional to the reflection coefficient for normal incidence (perpendicular to the $z$ axis), ignoring the reverberation term will eliminate the reverberations of normal-incident events (flat-bed reflections) and attenuate the reverberations of dipping events.

As was mentioned earlier in this chapter, the solution of the LITWEQ contains both upcoming and downgoing waves. However, when the medium velocity is constant (hence, the impedance is constant, because the density is constant in the acoustic wave equation), LITWEQ migration will not generate reverberations on the final section. The reverberation-free solution of the LITWEQ, in a constant-velocity medium, can be seen from the impulse response of the LITWEQ operator shown in Figure 3.3a.

When the velocity function has a discontinuity at some depth, the waves extrapolated to that position will be transmitted and also reflected, generating reverberations. The reverberation can be reduced if we ignore the reverberation term represented by equation (3.34). Figure 3.5 shows the difference between ignoring and adding the reverberation term in LITWEQ migration. The model has a sharp velocity discontinuity at $\tau = 18$ [$v(\tau<18) = 2$ and $v(\tau\geq 18) = 4$, in normalized units]. The input data is a spike at ($t = 28$, $x = 33$). The reverberation appears as the concave-down curve in the

middle of the figures and is marked by $M$.

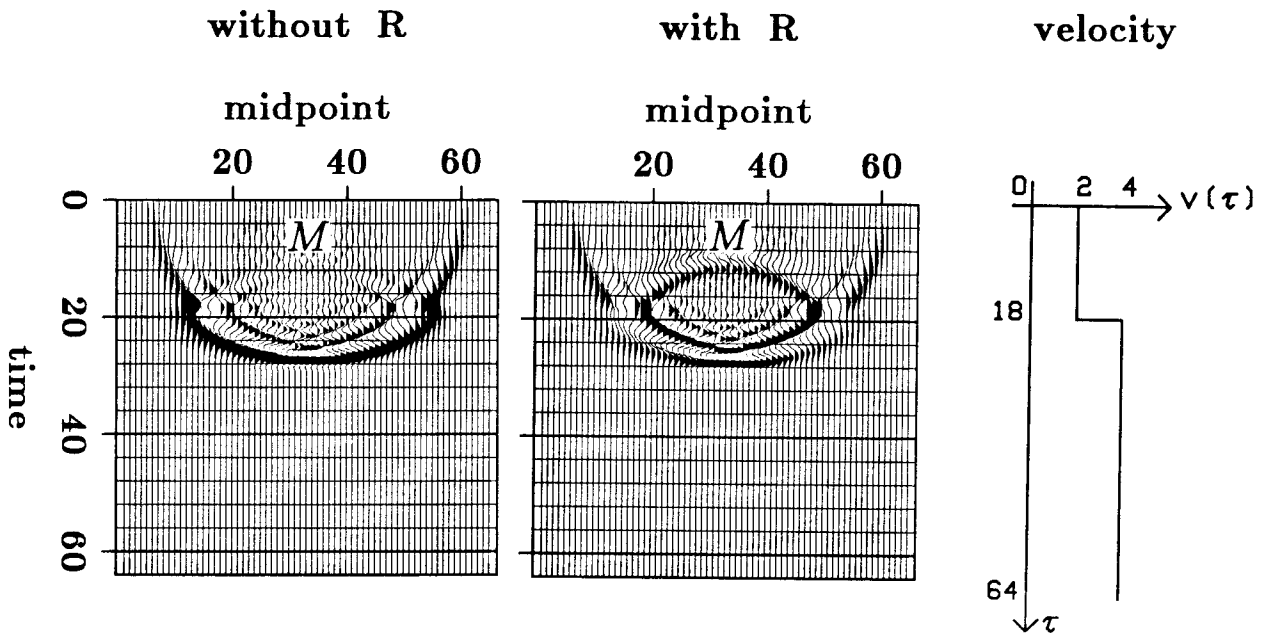


FIG. 3.5. Significance of the reverberation term in generating reverberations from a velocity discontinuity in LITWEQ migration. $R$ is the reverberation term defined in equation (3.34). The reverberations of the normal incidence are eliminated completely, while the reverberations of the non-normal incidence are attenuated, when ignoring the reverberation term.

The finite-difference LITWEQ algorithm coded with both the reverberation term and the time-shifting term can be used in modeling both primary and multiple reflections in variable velocity media.

**Why use the LITWEQ method?**

This section, together with the preceding sections, has formulated the basics of the linearly transformed wave equation method. The advantages and disadvantages of using this method, compared with other two-way wavefield extrapolation methods, will now be summarized.

The 2-D LITWEQ method extrapolates a wavefield nearly along the characteristic lines of wave propagation. The closer the direction of wavefield extrapolation to the characteristic lines, the more stable and accurate the result will be. Conventional two-way wavefield extrapolation methods, such as the reverse time method, calculate wavefields along either the $t$ axis or the $z$ axis, both of which are far from the

characteristic lines. The LITWEQ method offers a more stable and accurate finite-difference scheme than conventional two-way wavefield extrapolation methods in either $(x\,,\,z\,,\,t\,)$ or $(x\,,\,\tau,\,t\,)$ coordinates.

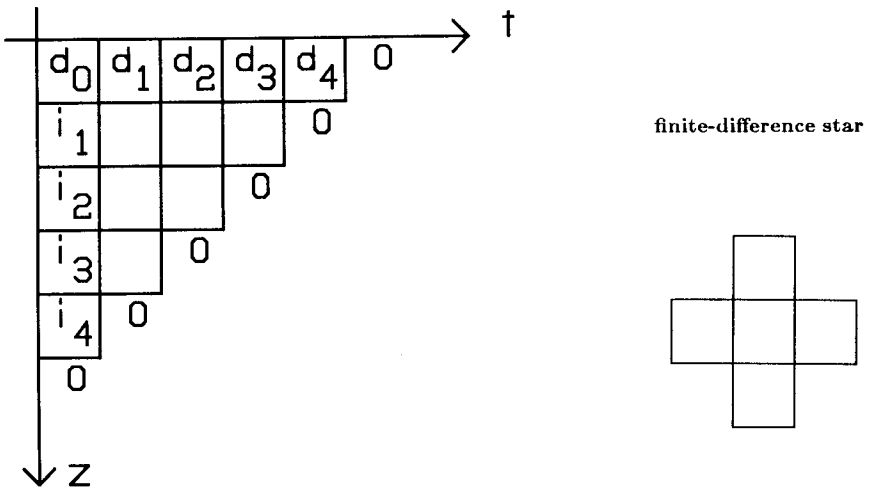


FIG. 3.6. The finite-difference grids and the star pattern of a second-order reverse time migration in the $(t\,,\,z\,)$ plane.

Figure 3.6 shows the finite-difference grids and the star pattern of a second-order reverse time migration. Comparing Figures 3.1 and 3.6, we see that the finite-difference grids in $(t_1,\,t_2)$, after transformation, are reduced to $1/\sqrt{2}$ of their original sizes in $(t\,,\,\tau)$. This is another factor in improving the accuracy of the LITWEQ method (without reducing the time-sampling interval in input seismic data as required by other finite-difference methods). Figures 3.7a and 3.7b compare impulse responses of both LITWEQ and reverse time migrations. The LITWEQ migration gives more accurate and less dispersive result than the reverse time migration. Field data results of applying these two migration schemes will be shown in the next section. Another advantage is that the LITWEQ method simplifies computation by transforming the conventional

three-level, five-point star pattern in $(t\,,\,\tau)$ into a two-level, four-point finite-difference star pattern in $(t_1,\,t_2)$.

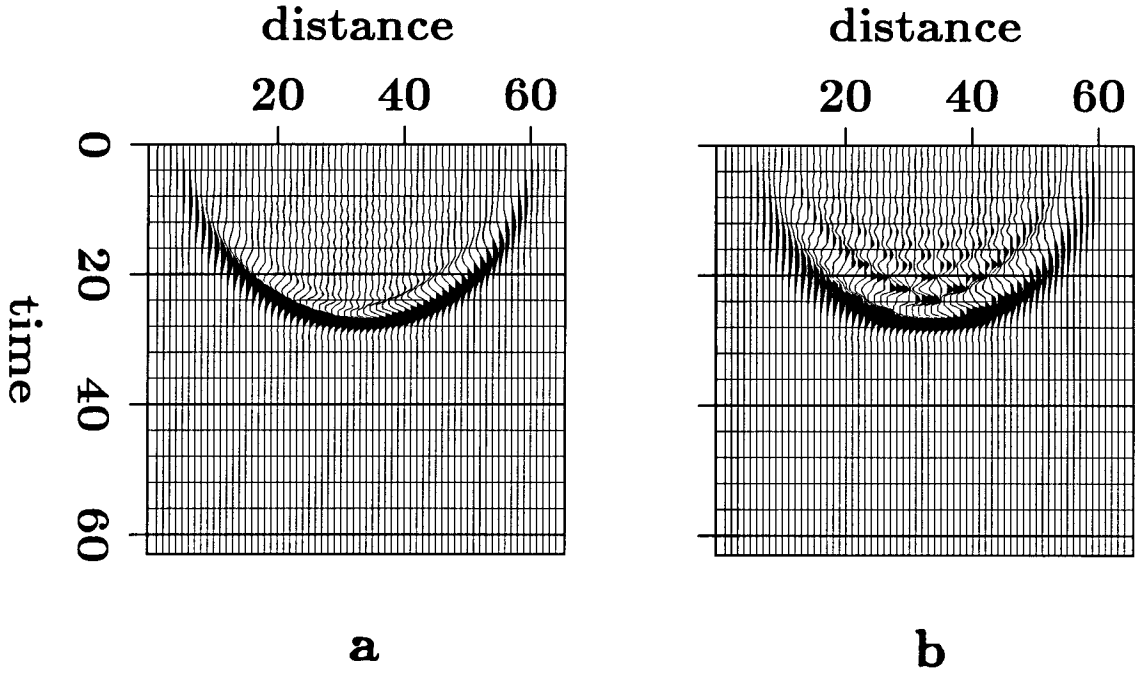


FIG. 3.7. **a.** An impulse response of a LITWEQ migration. **b.** An impulse response of a reverse time (second-order leap-frog) finite-difference migration. Plotting parameters for both figures are same. The semicircle is more accurately imaged in **a** than in **b**. Notice also the dispersions are more severe in **b** than in **a.**

One disadvantage, though, is that the computational cost for the LITWEQ method is twice that of conventional methods. Also, for the purpose of modeling, the $(x\,,\,z\,,\,t\,)$-domain reverse time method may be more direct and easier to use than the $(x\,,\,t_1,\,t_2)$-domain LITWEQ method, because physical parameters for modeling are usually given as functions of $(x\,,\,z\,)$.

The 2-D LITWEQ method is still not a perfectly characteristic method. Ray tracing of wavefronts may be needed to determine the characteristic directions of wave propagation at any particular time. Irregular grid sizes and different orientations of the finite-difference operator would be expected as the time changes.

## § 3.6 APPLYING THE LITWEQ MIGRATION TO FIELD DATA

The general purpose of migration is to migrate both diffractions and dipping-bed reflections. Several factors are considered in deciding which algorithm to use for migrating a stacked section: economy of computation, the particular purpose of the migration, the quality of the stacked section, and the geology of the section. No migration is needed if the section has only flat-bed reflections and no lateral velocity variations. Algorithms employing lower-order approximate equations can be used if no steeply dipping reflections are present in the stacked section. Steep-dip events can be preserved better in stacked sections if dip-moveout, or constant-velocity stack algorithms, are used. LITWEQ migration can give better results than lower-order-equation migrations if the seismic data are recorded over an area where the geology is complicated and if the steep-dip reflections are well stacked into the stacked sections.

The input seismic sections in the following two field data examples contain steep-dip reflections from some fault planes and salt-dome boundaries in the Gulf of Mexico. These reflections are imaged well by LITWEQ migration.

### Normal-fault dataset

Both LITWEQ migration and conventional 15-degree migration were performed on a dataset from the Gulf of Mexico. The input dataset is a stacked section that has both flat-bed reflections and steeply dipping fault-plane reflections. To give a closer view of the migration results, the stacked section and the two migrated sections are windowed, as shown in Figures 3.8a, 3.8b and 3.8c, respectively.

For both the 15-degree and the LITWEQ migrations, a few traces at each side of the input data were tapered slightly so that the reflections from the edges of the finite-differencing grids are reduced.

Diffraction tails in the unmigrated section are collapsed into diffracting points in both the migrated sections shown in Figures 3.8b and 3.8c. The fault-plane reflection between horizontal coordinates 7.9 and 10 km, at about 1.8 to 3 s, is better migrated and preserved by the LITWEQ method than by the 15-degree one. In the section migrated with the 15-degree equation the upper part of this fault-plane reflection is almost lost, because it has a larger angle than the lower part, and the 15-degree method does not handle the steep-dip reflection properly. The difference between these two migrated sections can be seen more clearly by subtracting the two migrated sections (Figure 3.8d). It is actually the low-pass-dipfiltering of the 15-degree operator that eliminates the higher-angle reflection. The 15-degree-equation migration also tends

to undermigrate the dipping events. Some undermigrated fault-plane reflections on both the migrated sections are possibly caused by the out-of-plane reflections at those positions. A three-dimensional algorithm should migrate them properly.

For comparison, a phase shift migration is applied to the stacked section. Phase shift migration is accurate in imaging reflections with dips from 0 to 90 degrees: therefore, the steeply dipping fault plane is also imaged well in Figure 3.8e, which further confirms the existence of the steeply dipping fault plane marked by $E$ in Figure 3.8c. However, one disadvantage of phase shift migration, as seen in the lower part of Figure 3.8e, is that migration artifacts are strong in the migrated section due to wraparound effects of Fourier transformation and due to poor performance of Fourier methods when input data have low signal-to-noise ratio.

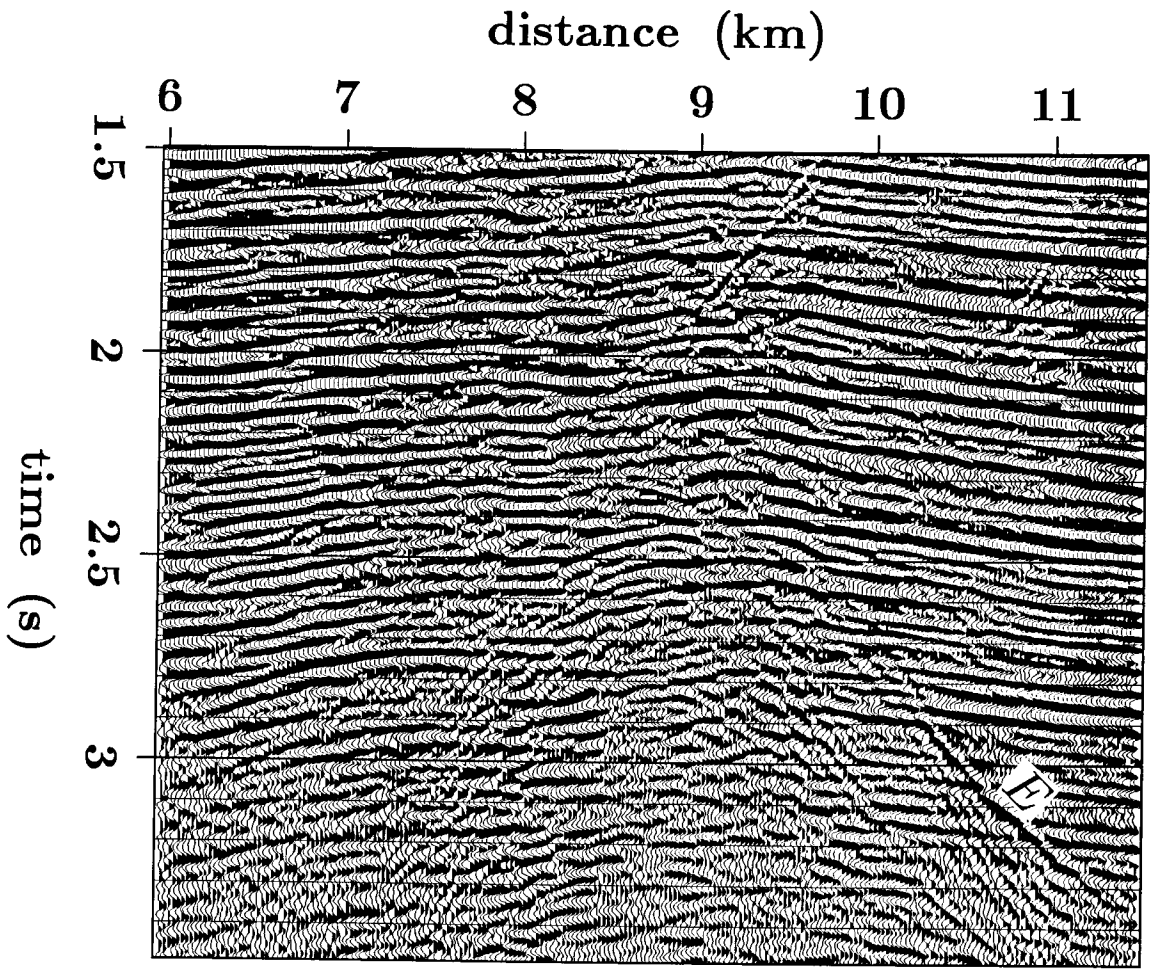


FIG. 3.8a. A window of an unmigrated section of a normal fault dataset from the Gulf of Mexico. The horizontal distance spacing is 25 m. The time spacing in the sections is 0.008 s.

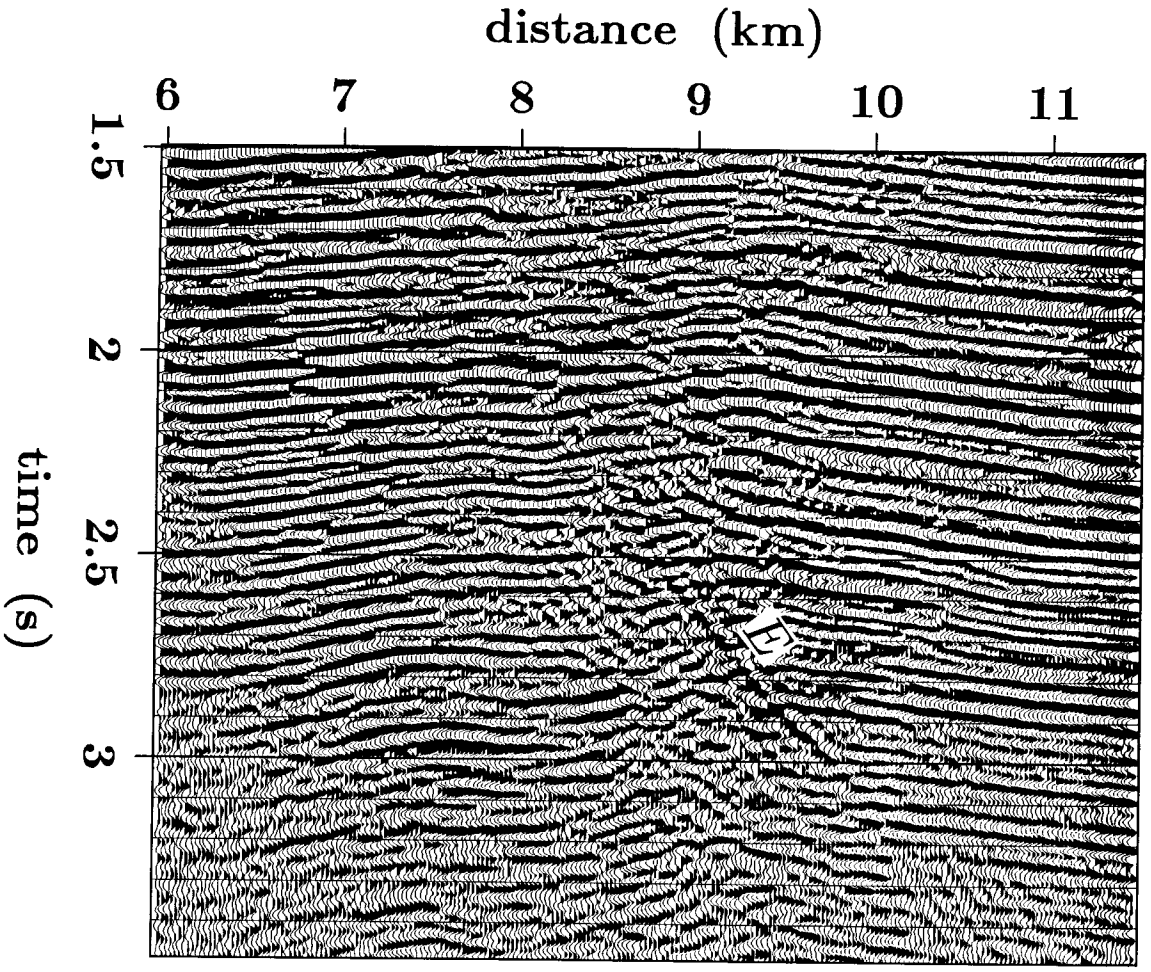


FIG. 3.8b. Migrated section using the 15-degree wave equation. The upper part of the event marked by $E$ in Figure 3.8a has been eliminated in the migrated section (about 2 s to 2.5 s) by the dip-filter effect of the lower-order 15-degree migration operator.

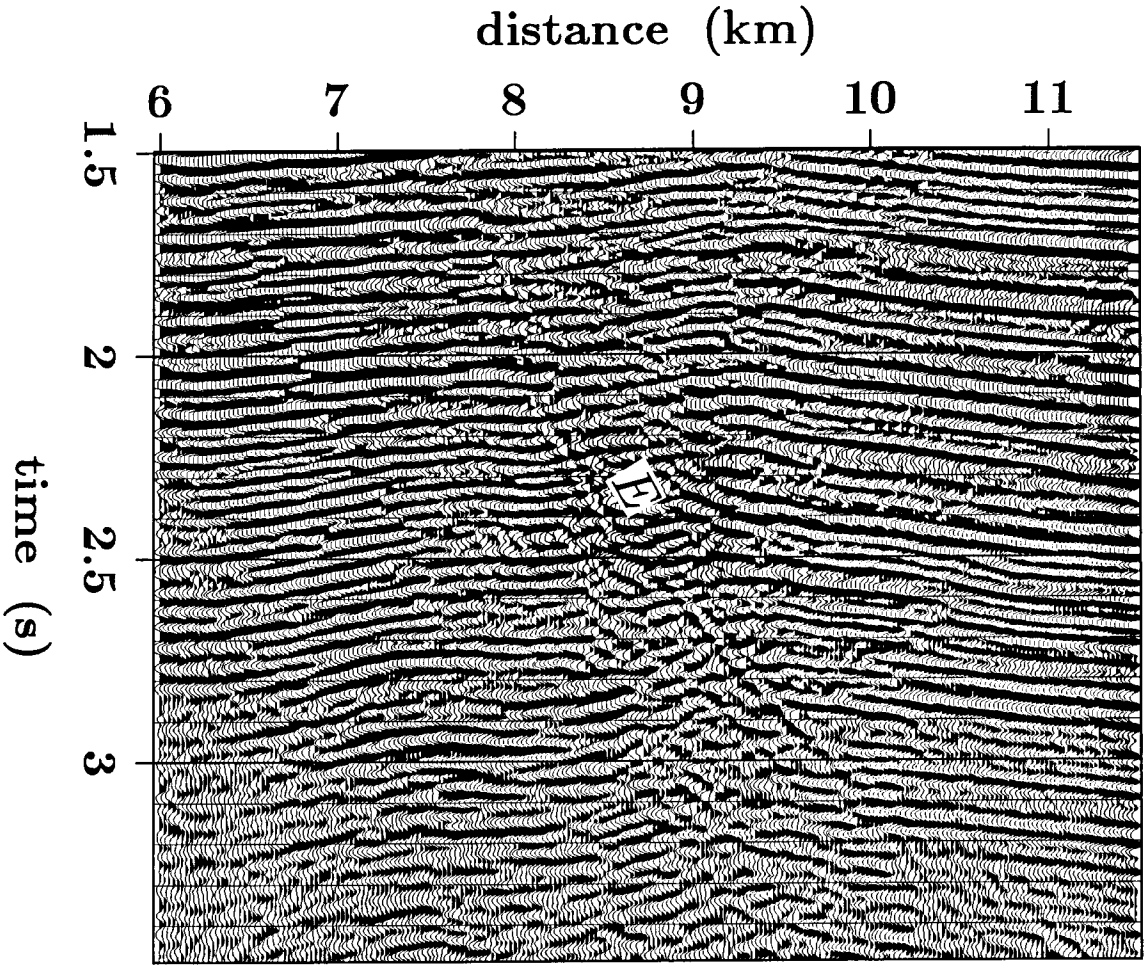


FIG. 3.8c. Migrated section using the LITWEQ. The event marked by $E$ is well preserved and migrated by the LITWEQ migration operator.

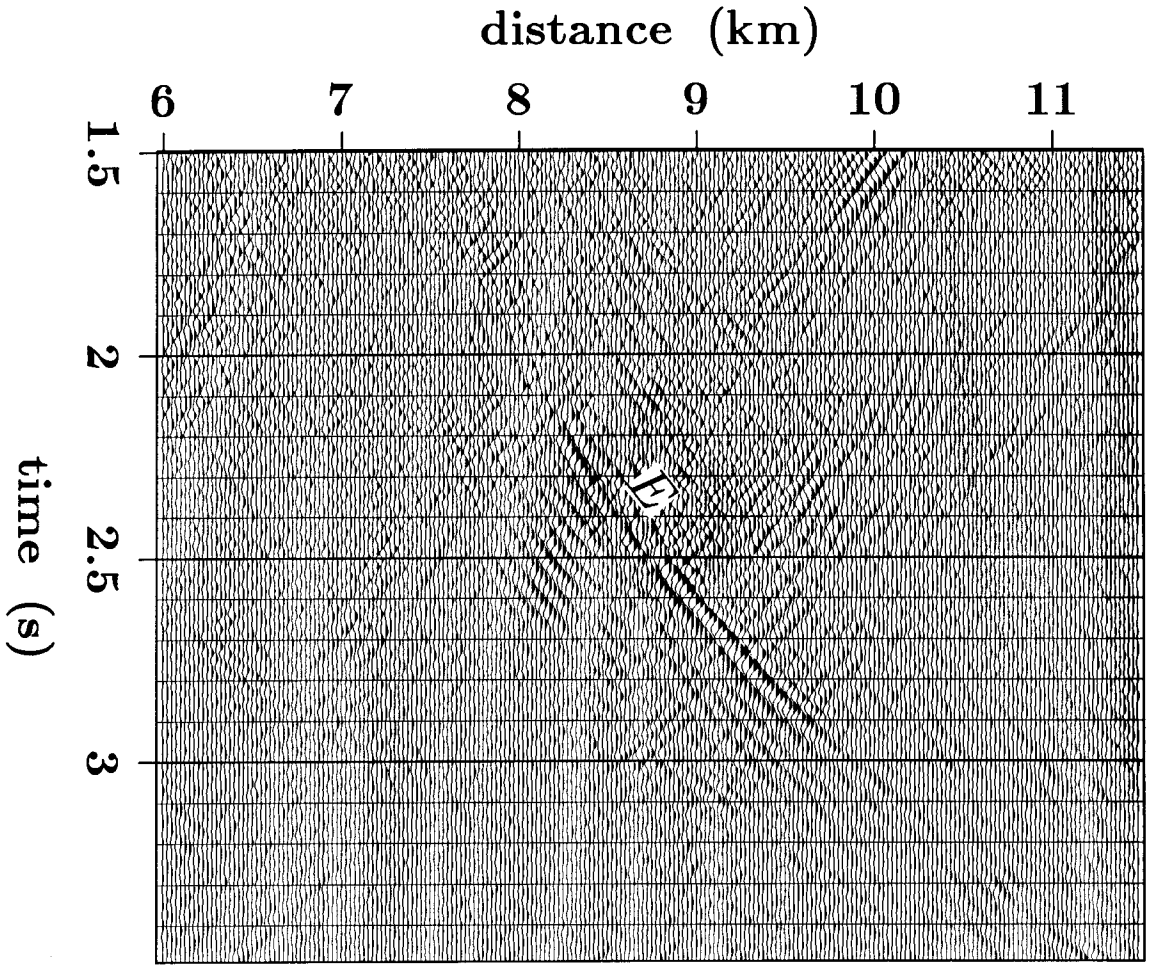


FIG. 3.8d. Difference between the two migrated sections (Figures 3.8b and 3.8c). The remaining fault-plane image (marked by $E$) shows again that the LITWEQ migrates the fault-plane reflections properly, while the 15-degree equation suppresses the image of the fault plane.

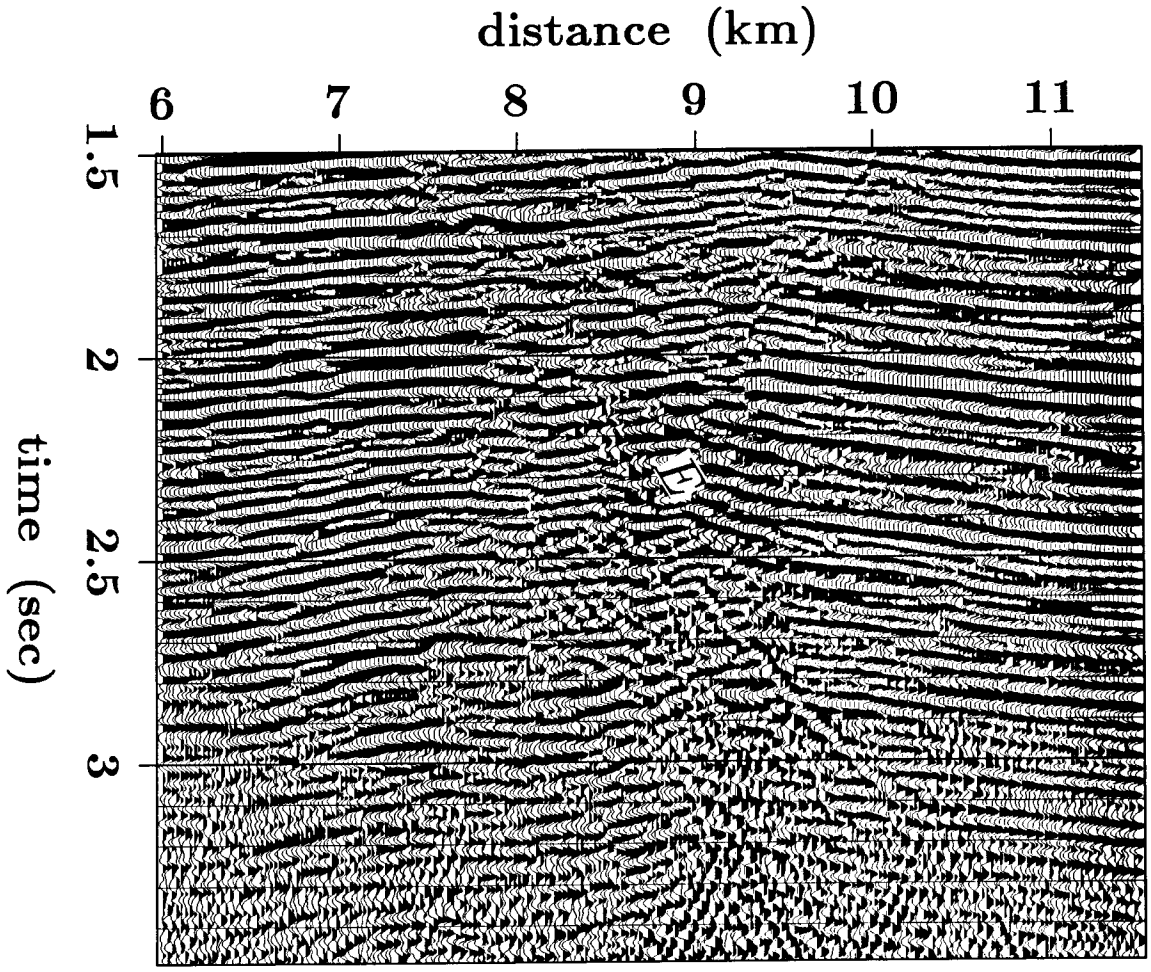


FIG. 3.8e. Section migrated using a phase shift method. The steeply dipping fault plane is imaged, while migration artifacts generated by wraparound effects of Fourier transformation obscure the images at the bottom of the section.

**Salt-dome dataset**

The salt-dome dataset is a CMP-stacked section (Figure 3.9a) of a survey line in the Gulf of Mexico. The sample interval is 0.004 s, and the midpoint interval is 25 m. The geologic structure under the line is a mushroom-shaped salt dome with surrounding sediments. A velocity function for migrating the section is obtained by smoothing the interval velocity profile obtained from a velocity analysis. The section is subsampled every 0.012 s. Four migration methods are applied to the dataset using the same migration velocity function. These are the 15-degree wave equation, the 45-degree wave equation, the LITWEQ and the second-order reverse time. The results are shown in Figures 3.9b, 3.9c, 3.9d and 3.9e, respectively.

The input stacked section contains steep-dip reflections from the salt-dome boundary. Because the conventional 15-degree method tends to undermigrate and distort the dipping events, the salt dome is poorly imaged (Figure 3.9b). Even with the higher-order 45-degree wave equation [$n$ =2 in equation (3.3)], the steep-dip reflections from the salt dome boundary are still under-migrated (Figure 3.9c). LITWEQ migration gives a better image of the salt dome, even managing to image reflectors greater than 90 degrees in the side of the salt dome with overhang (Figure 3.9d).

For comparison, a second-order reverse time migration is also applied to the salt-dome dataset. The section (Figure 3.9e) migrated by the reverse time method gives poorer and more dispersive image of the salt dome than the section (Figure 3.9d) migrated by the LITWEQ method, though both of them have located the boundaries of the salt dome. Figures 3.9b, 3.9c, 3.9d and 3.9e use the same plotting parameters.

To illustrate the correspondence of events in the migrated and stacked (unmigrated) sections, some intermediate results of the LITWEQ migration are shown in Figures 3.11a-3.11e. These results are obtained by slicing the ($x$ , $t$ , $\tau$) wavefield cube with certain surfaces. Figure 3.10 shows the intermediate data surfaces. The successive pictures in Figures 3.11a-3.11e show that the boundary of the mushroom-shaped salt dome is imaged as a result of the migration of the reflections and diffractions presented in Figure 3.11a, not as a result of migration artifacts. Another interesting phenomenon that can be observed from Figures 3.11a-3.11e is that the vertical streaks, or d.c. components, near the top of the salt dome (Figure 3.11e) are formed by migrating some water-bottom scattering waves with sediment velocities that are much higher than the water velocity. Band-pass filtering should be able to suppress the low-frequency streaks.

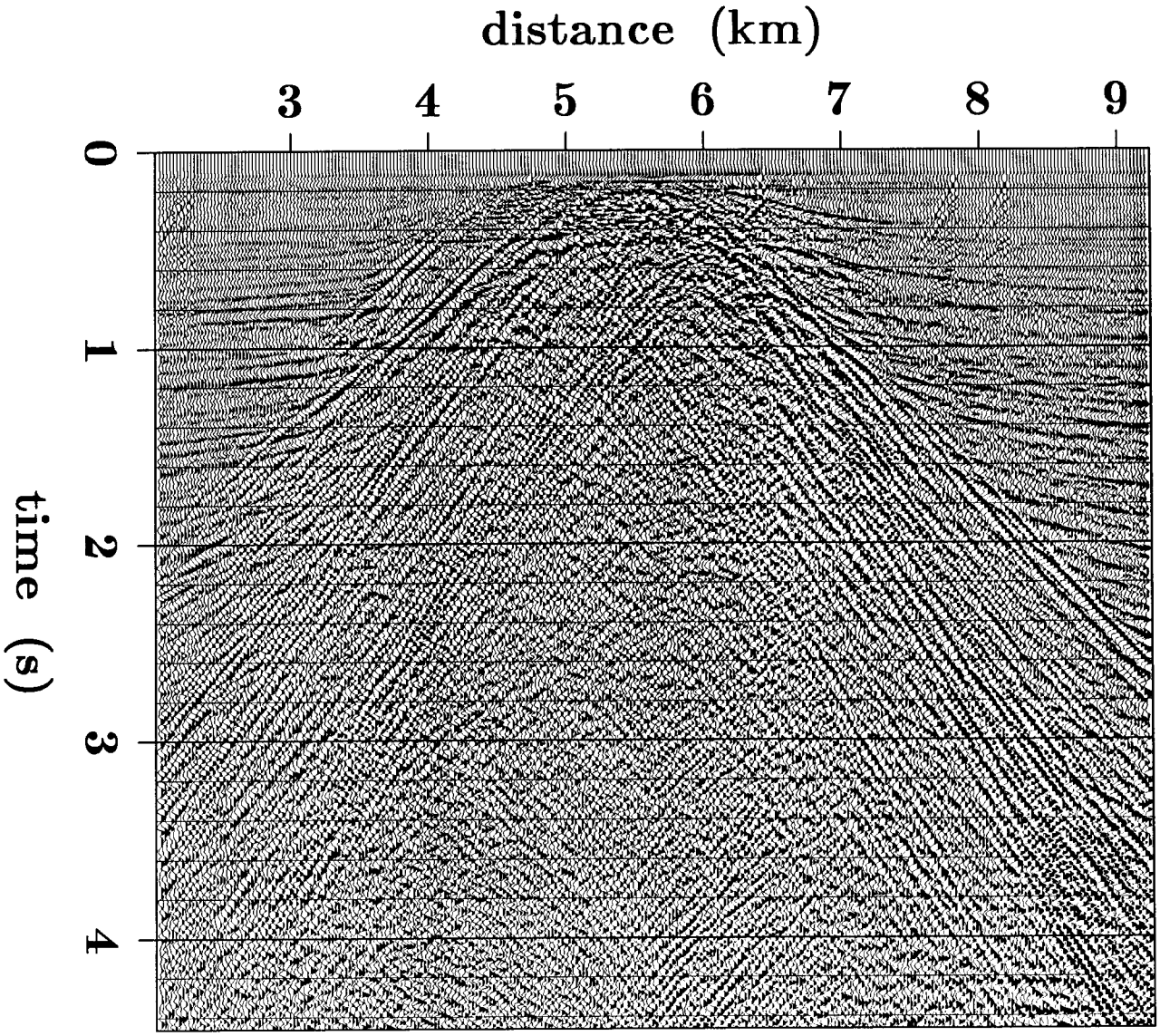


FIG. 3.9a. A stacked section of a survey line over a salt dome in the Gulf of Mexico.

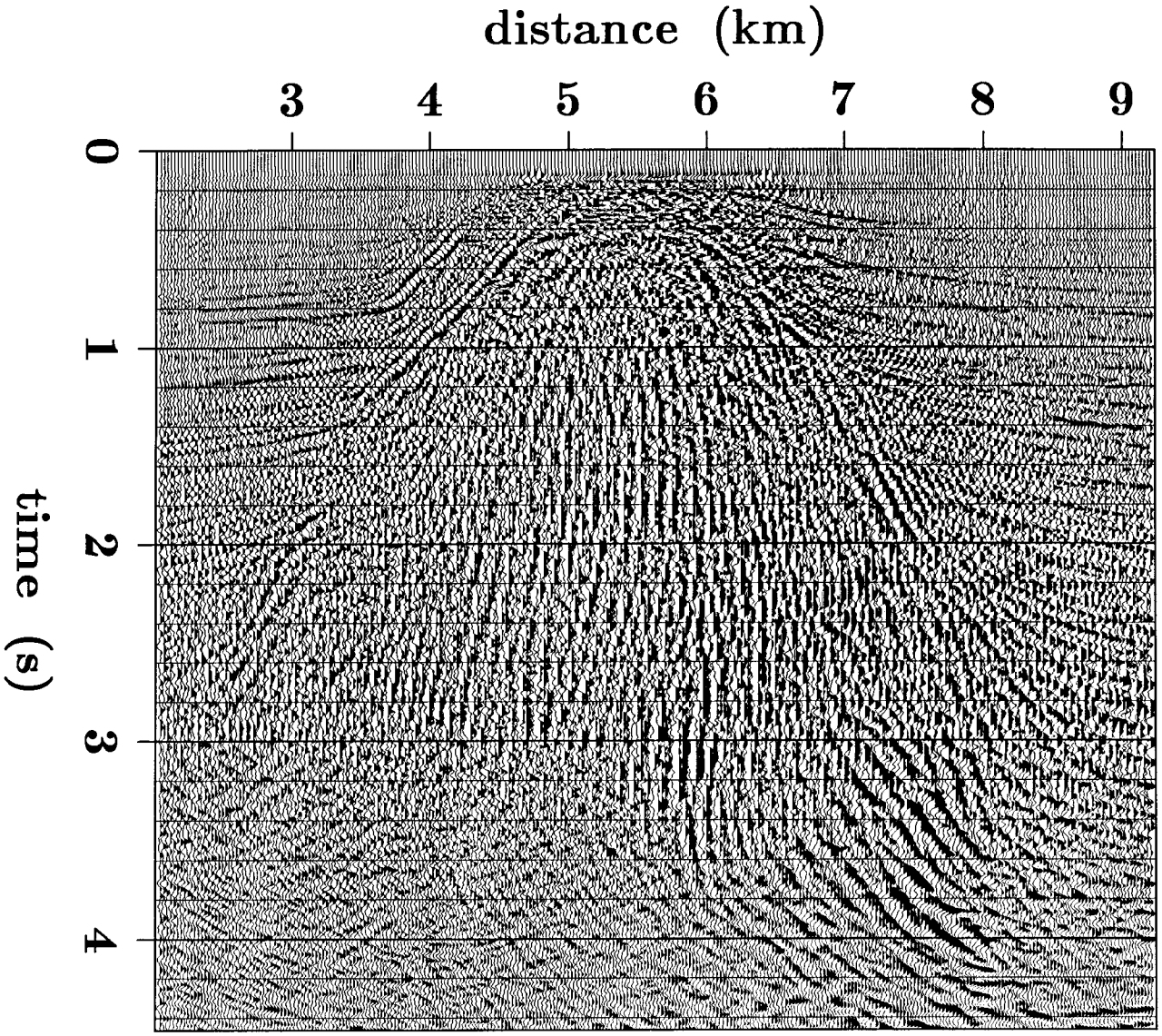


FIG. 3.9b. Section migrated using the conventional 15-degree wave equation. The salt-dome boundary is poorly resolved.

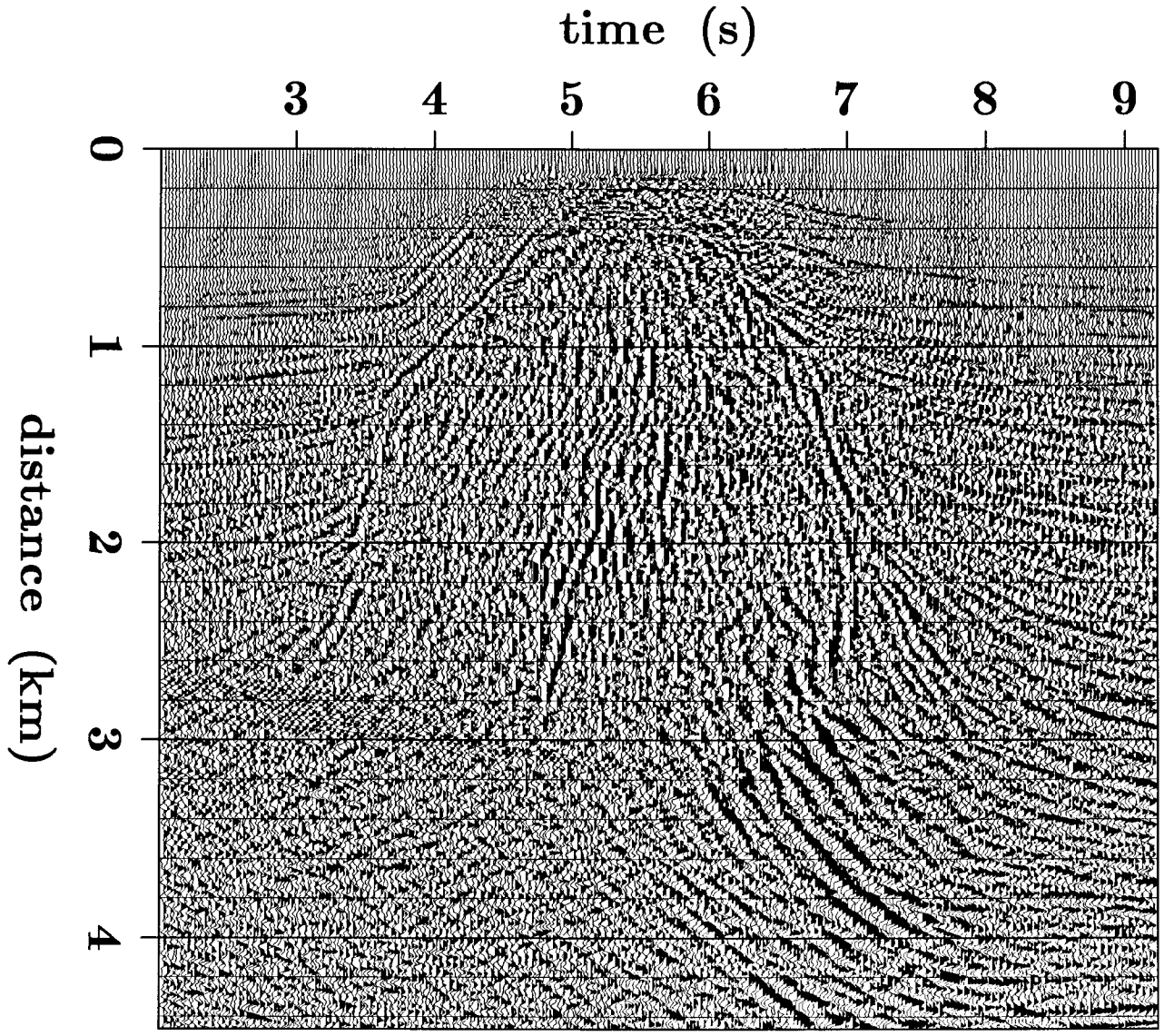


FIG. 3.9c. Section migrated using a 45-degree wave equation method. The boundary of the salt dome is better imaged than that in Figure 3.9b, because the higher-order equation is used. However, the steep-dip reflections from the salt dome boundary are still under-migrated.

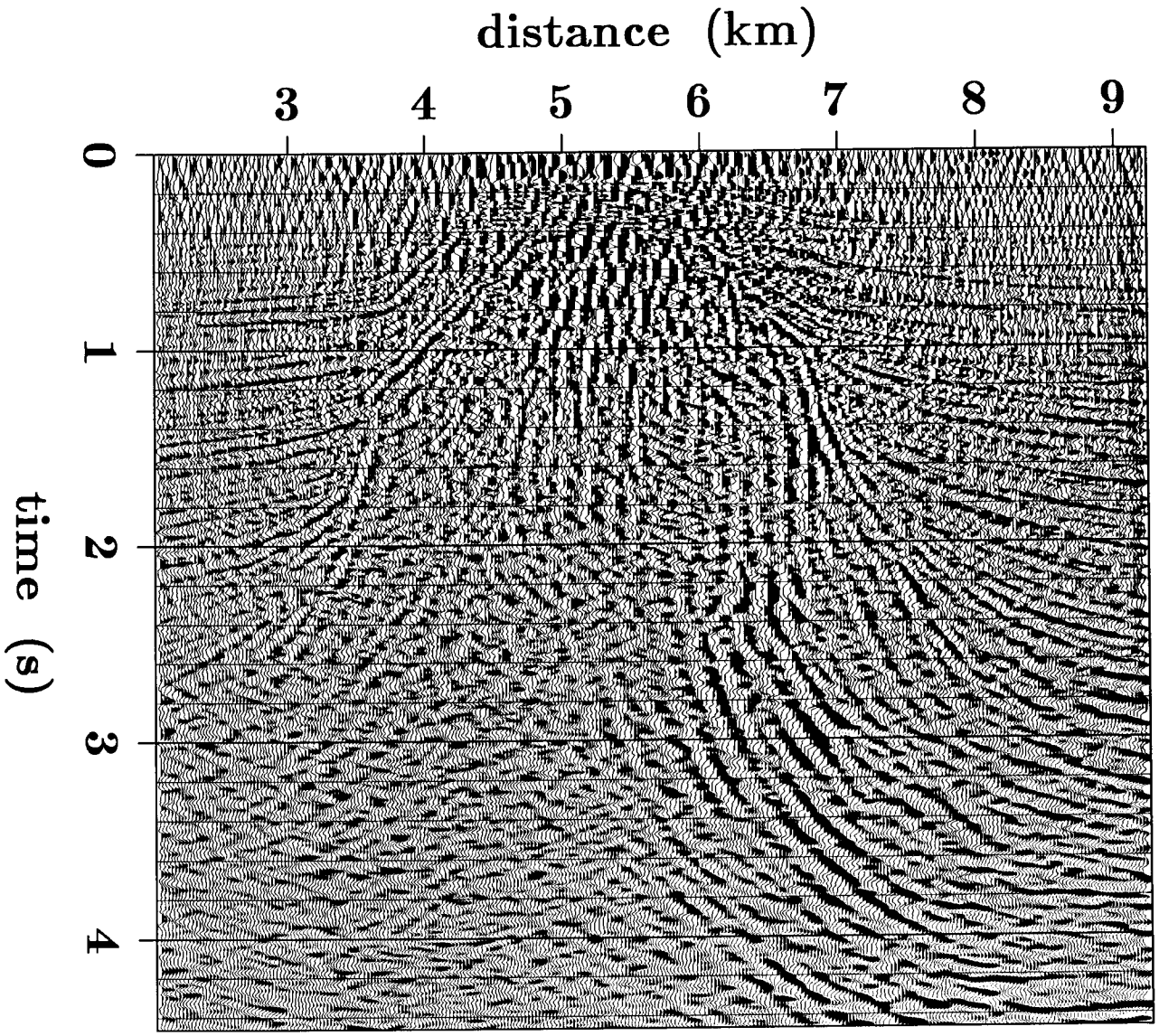


FIG. 3.9d. Section migrated using the LITWEQ. The boundary of the salt dome is well imaged.

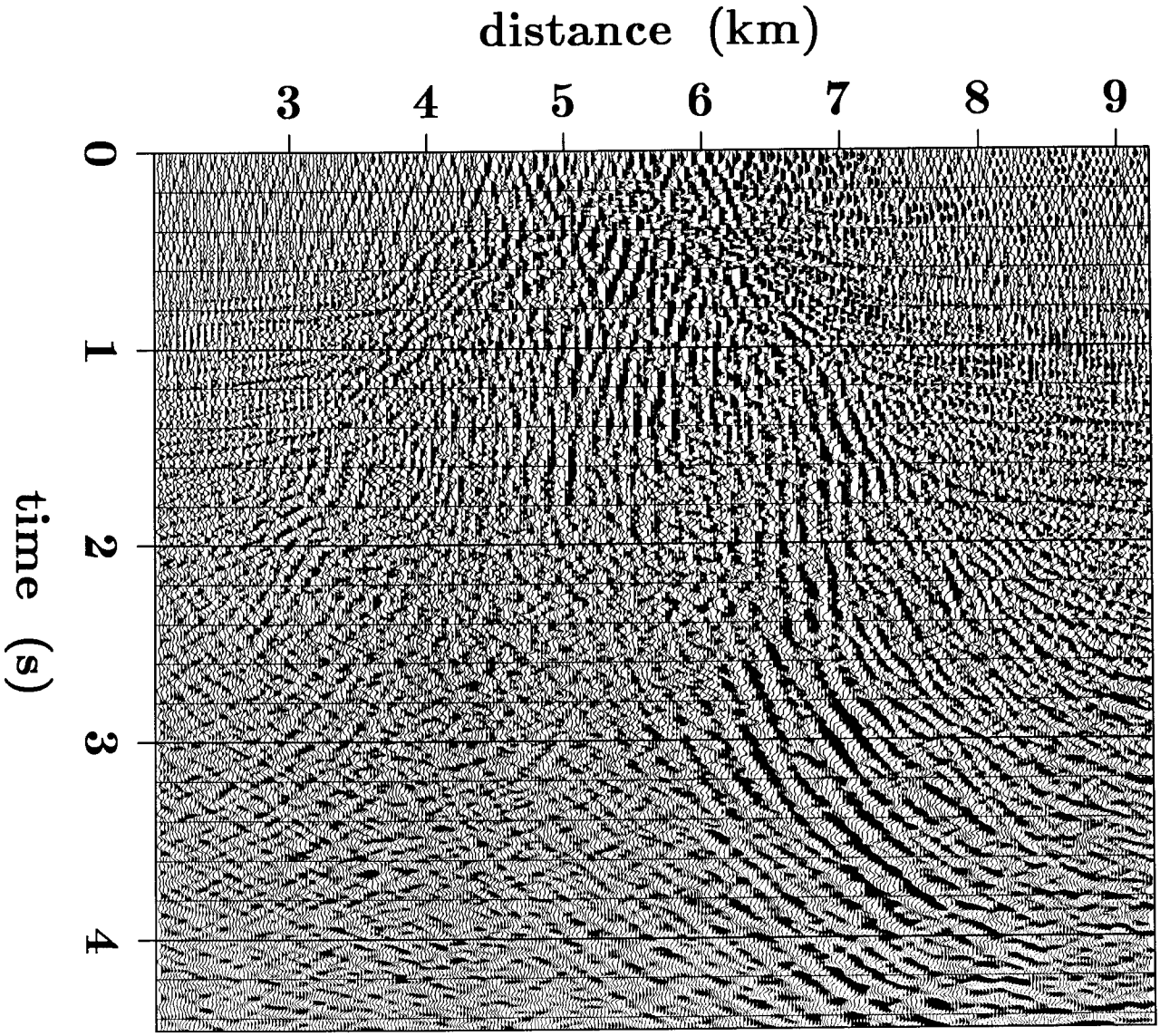


FIG. 3.9e. Section migrated using a second-order reverse time method. It gives less accurate and more dispersive image of the salt dome than the section (Figure 3.9d) migrated by the LITWEQ method.

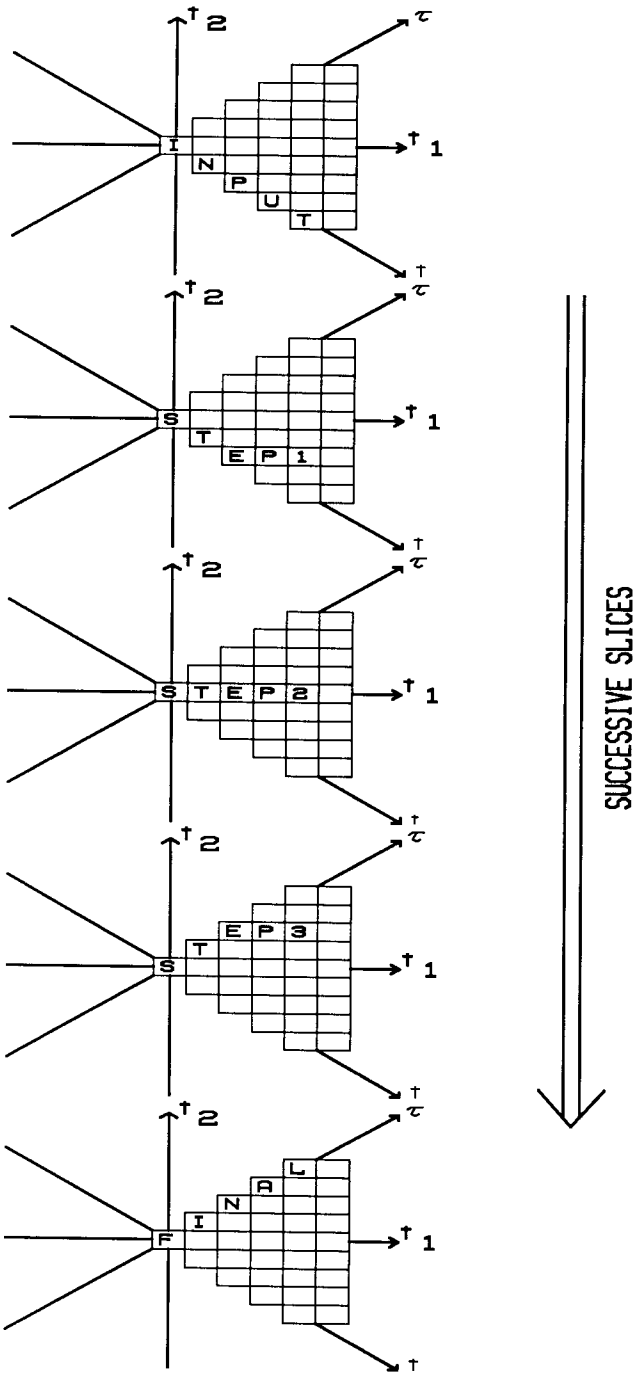


FIG. 3.10. Intermediate data surfaces of the LITWEQ migration. The third axis, $x'$, is perpendicular to the $(t_1, t_2)$ plane. The intermediate results are taken from the labeled boxes on the $(t_1, t_2)$ plane, as shown by the successive pictures in the figure.

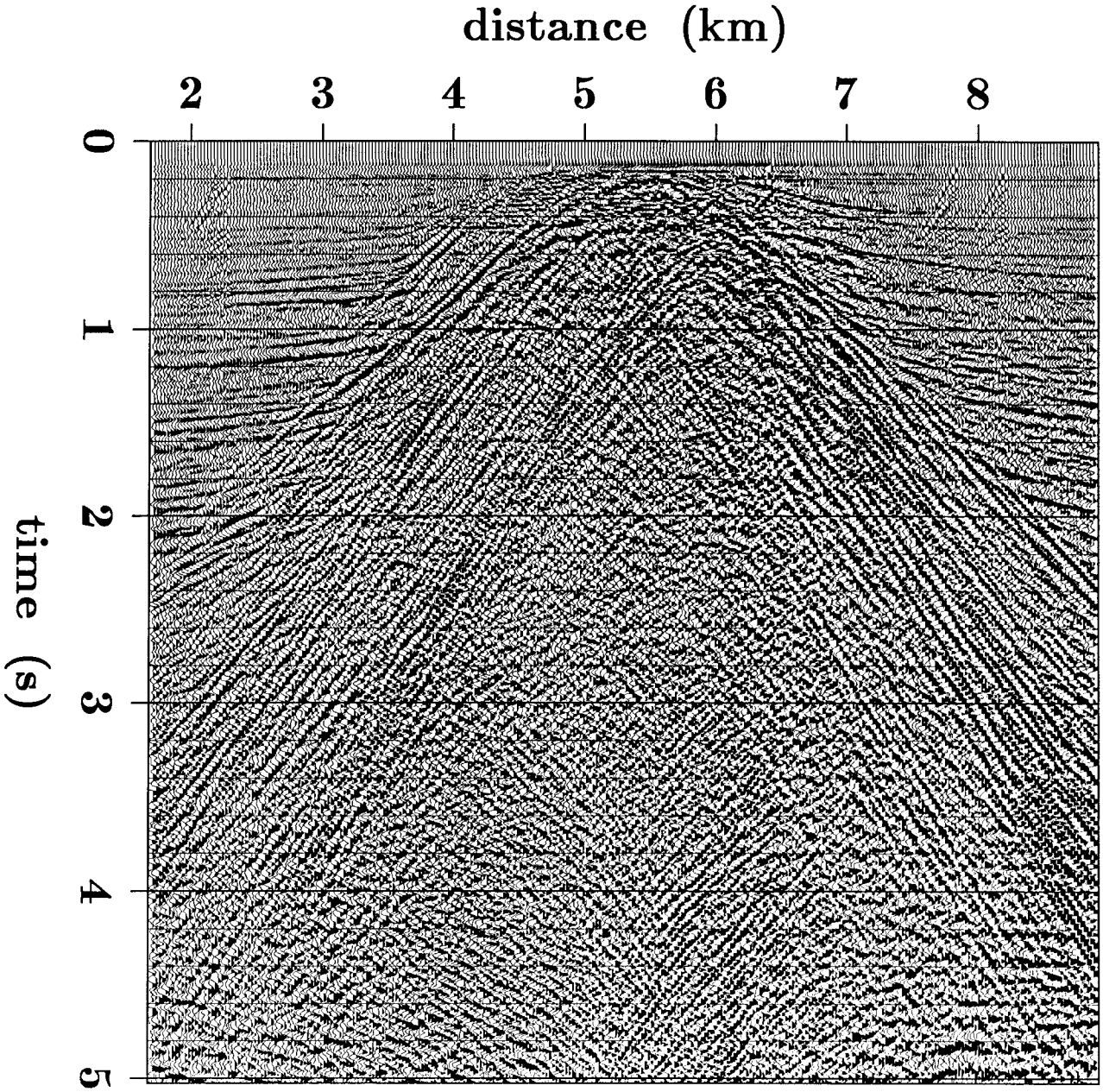


FIG. 3.11a. The stacked-section input of the LITWEQ migration.

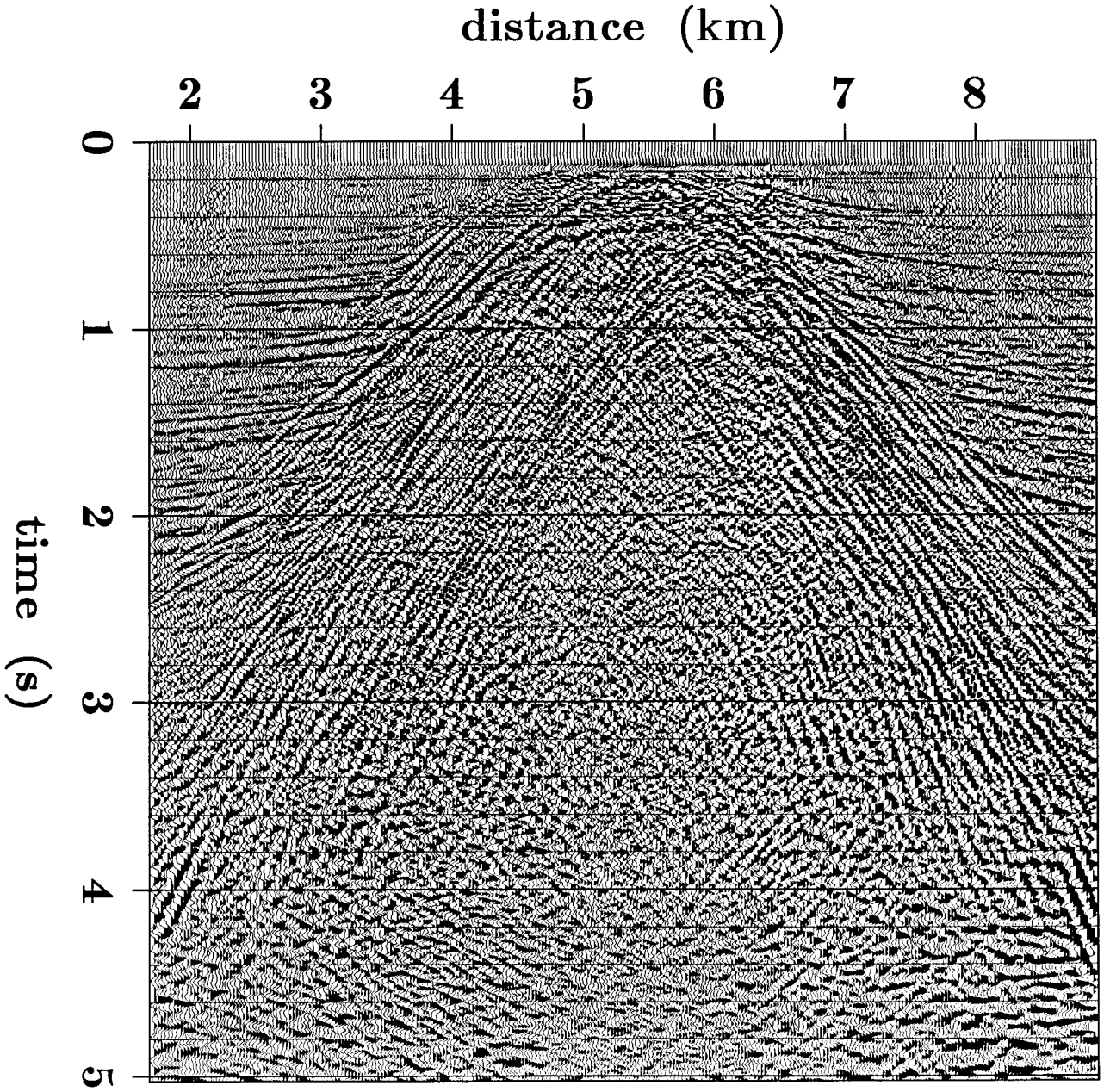


FIG. 3.11b. Intermediate step 1 of the LITWEQ migration. The dipping events begin to migrate upward.

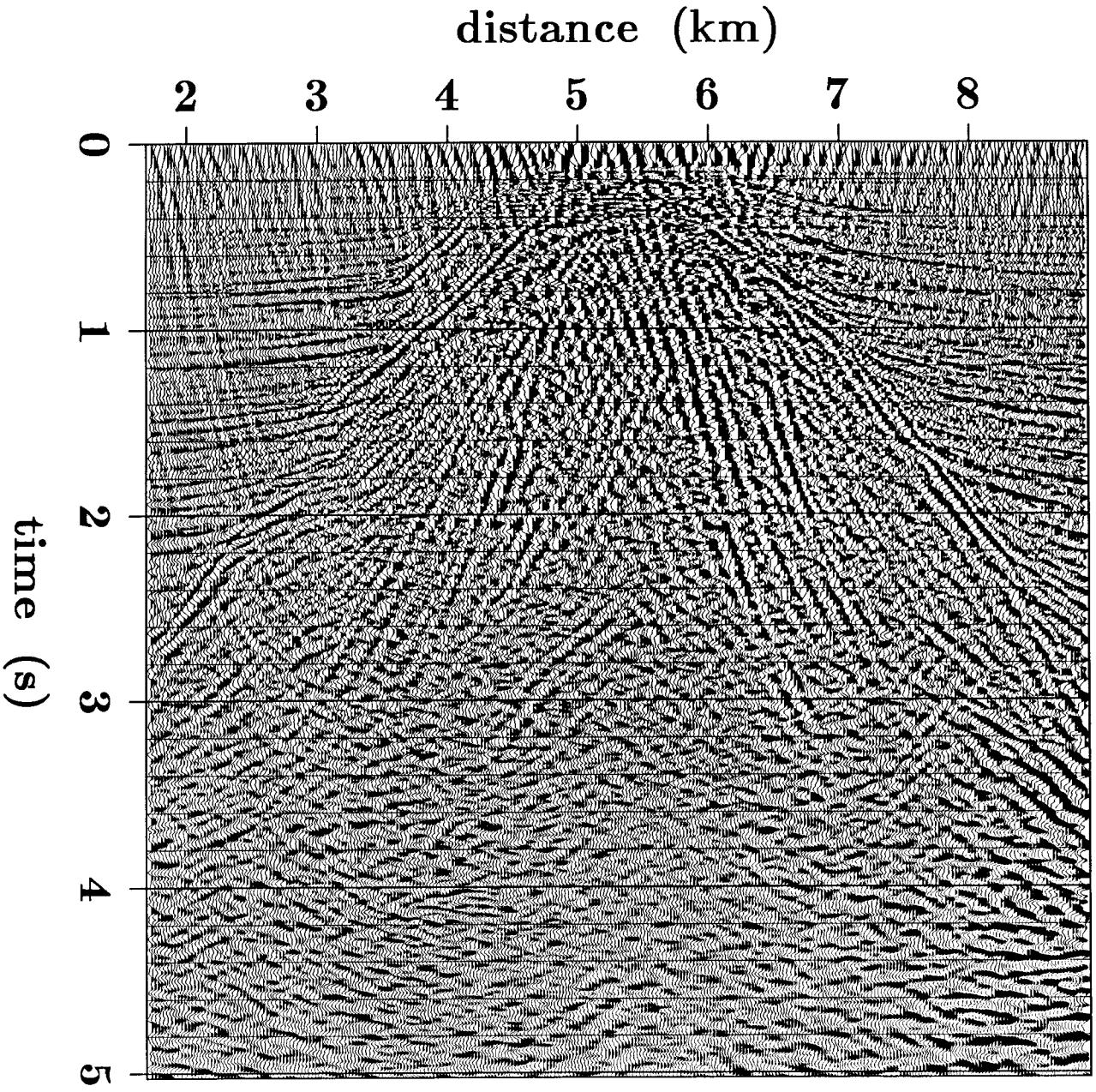


FIG. 3.11c. Intermediate step 2 of the LITWEQ migration. The dipping reflections from the salt-dome boundary are migrated further upward. Some water-bottom scattering events from the top of the salt dome migrate to the center of the dome.

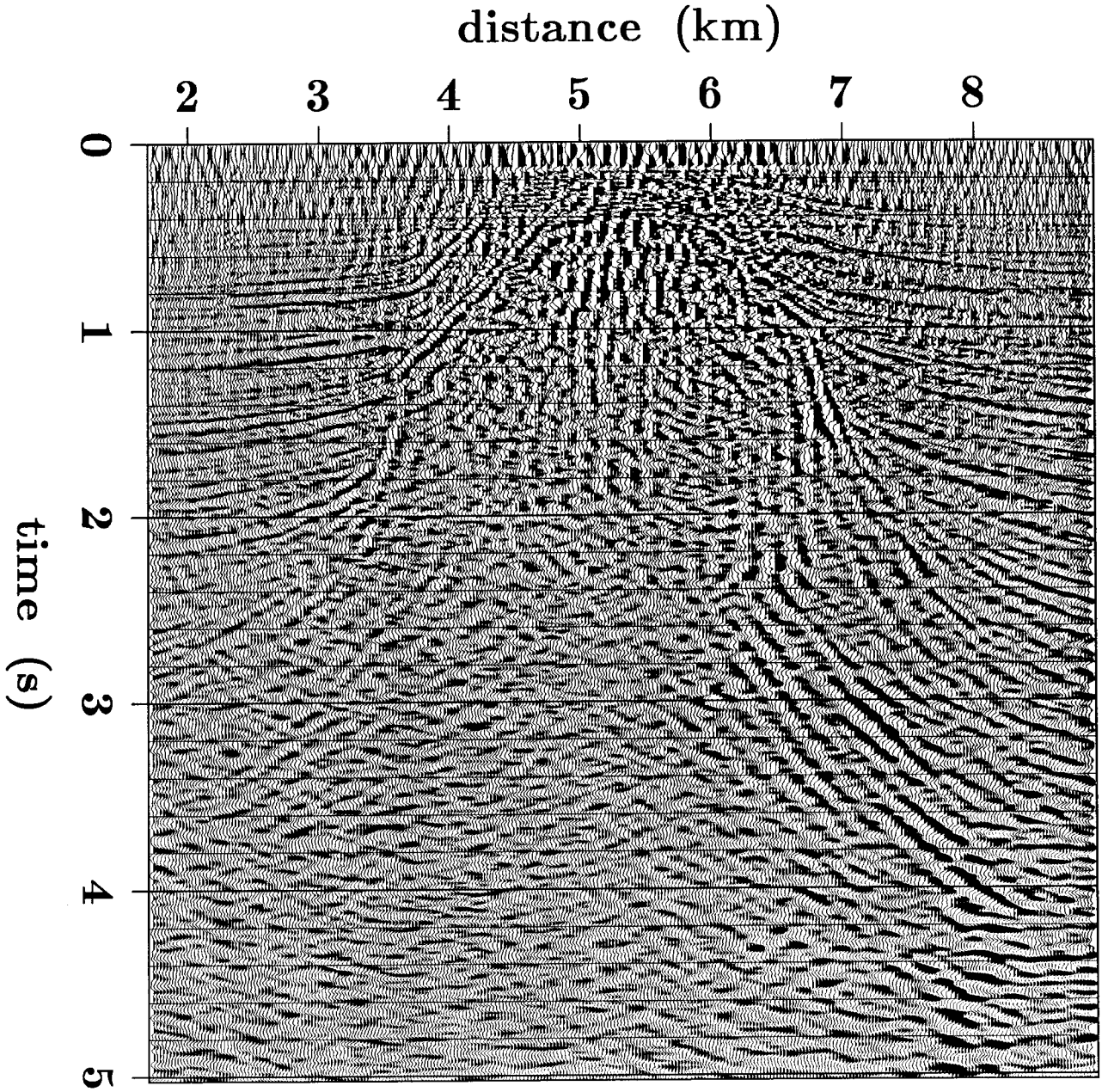


FIG. 3.11d. Intermediate step 3 of the LITWEQ migration. The salt-dome boundary starts to appear. The vertical streaks near the top of the dome are the water-bottom scattering events migrated with sediment velocities.

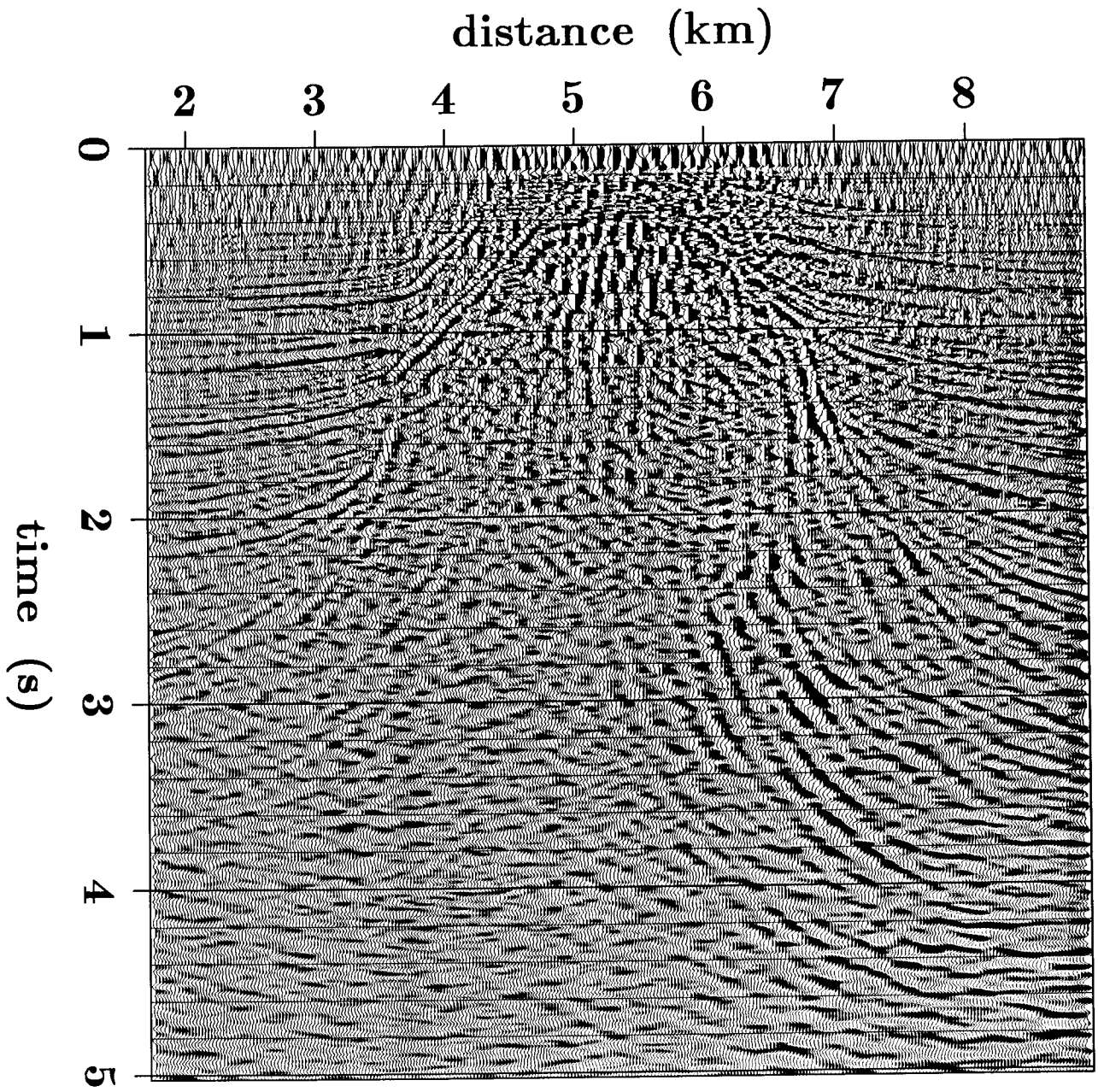


FIG. 3.11e. Final image of the geologic structure of the salt dome.

## § 3.7 SUMMARY

The LITWEQ equation is accurate for all events, regardless of their angles of propagation. The linear transformation over both depth and time reduces the two terms of the second derivative in the acoustic wave equation to a single second cross-derivative term in the LITWEQ, instead of dropping a second derivative as do both the retarded time coordinate transform $t' = t - z/v$, $z' = z$, and the moving coordinate transform $z' = z + vt$, $t' = t$ (Claerbout, 1976). The linear transformation is actually a combination of the retarded time and the moving coordinate transforms.

When velocity of medium is varying, a depth-to-time $(z-\tau)$ conversion of the scaler wave equation must be done before applying the velocity-independent linear transformation. The velocity-independent transformation gives a LITWEQ method with uniformed spaced intervals in the transformed coordinates $(t_1, t_2)$.

The linear transformation gives us an accurate wavefield extrapolation operator that can be applied not only to stacked data migration, but also to both primary- and multiple-reflection modeling, prestack migration, three-dimensional wavefield extrapolation, wave-equation inversion and seismic tomography, all of which will be discussed in the next two chapters.